

000 001 SCALING LAWS AND SPECTRA OF SHALLOW NEURAL 002 NETWORKS IN THE FEATURE LEARNING REGIME 003 004

005 **Anonymous authors**

006 Paper under double-blind review

007 008 ABSTRACT 009

011 Neural scaling laws underlie many of the recent advances in deep learning, yet
012 their theoretical understanding remains largely confined to linear models. In this
013 work, we present a systematic analysis of scaling laws for quadratic and diagonal
014 neural networks in the feature learning regime. Leveraging connections with
015 matrix compressed sensing and LASSO, we derive a detailed phase diagram for the
016 scaling exponents of the excess risk as a function of sample complexity and weight
017 decay. This analysis uncovers crossovers between distinct scaling regimes and
018 plateau behaviors, mirroring phenomena widely reported in the empirical neural
019 scaling literature. Furthermore, we establish a precise link between these regimes
020 and the spectral properties of the trained network weights, which we characterize
021 in detail. As a consequence, we provide a theoretical validation of recent empirical
022 observations connecting the emergence of power-law tails in the weight spec-
023 trum with network generalization performance, yielding an interpretation from
024 first principles.

025 1 INTRODUCTION

027 A central development in modern deep learning has been the recognition that neural network gen-
028 eralization does not improve unboundedly when training data, model size, or compute are scaled in
029 isolation. Instead, extensive empirical evidence reveals the presence of performance bottlenecks un-
030 less these resources are increased together (Kaplan et al., 2020; Brown et al., 2020; Hoffmann et al.,
031 2022). Characterizing these trade-offs, and in particular predicting the resulting *neural scaling laws*,
032 has emerged as a fundamental challenge for deep learning research, with significant implications for
033 the design of efficient and resource-conscious models.

034 Our goal in this work is to investigate this question in the context of shallow neural networks. More
035 precisely, consider the following supervised empirical risk minimization (ERM) problem for the
036 class of two-layer neural networks $f(\mathbf{x}; \mathbf{W}, \mathbf{a}) = \mathbf{a}^\top \sigma(\mathbf{W}\mathbf{x} + \mathbf{b})$:

$$037 \min_{\mathbf{W}, \mathbf{a}} \sum_{\mu=1}^n (y_\mu - f(\mathbf{x}_\mu; \mathbf{W}, \mathbf{a}))^2 + \lambda (\|\mathbf{W}\|_F^2 + \|\mathbf{a}\|_2^2) \quad (1)$$

040 where $\mathbf{W} \in \mathbb{R}^{p \times d}$ and $\mathbf{a} \in \mathbb{R}^p$ are the first- and second-layer weights, respectively. Although
041 substantial progress has been achieved in recent years, our current understanding of scaling laws
042 for the generalization performance of the ERM minimizer in eq. (1) remains largely confined to the
043 random features regime (Bahri et al., 2024; Maloney et al., 2022; Paquette et al., 2024; Atanasov
044 et al., 2024; Bordelon et al., 2024; Kunstner & Bach, 2025). In this setting, the problem reduces to
045 a kernel method, where scaling behavior has been classically studied, and is known as *source and*
046 *capacity conditions* (Caponnetto & De Vito, 2007; Cui et al., 2021; Defilippis et al., 2024).

047 In this work, we move beyond the random features regime and investigate neural scaling laws for
048 the ERM minimizer in eq. (1) in the teacher-student setting. That is, we assume that the target task
049 is generated by a teacher network of the same architecture

$$051 y_\mu = f(\mathbf{x}_\mu; \mathbf{W}^*, \mathbf{a}^*) + \sqrt{\Delta} \xi_\mu, \quad (2)$$

052 where $\{\mathbf{x}_\mu\}_{\mu=1}^n \stackrel{i.i.d.}{\sim} \mathcal{N}(0, I_d)$ denotes the dataset and $\{\xi_\mu\}_{\mu=1}^n \stackrel{i.i.d.}{\sim} \mathcal{N}(0, 1)$ is an additive Gaus-
053 sian label noise with variance $\Delta \geq 0$. The statistics of the target weights $\mathbf{W}^*, \mathbf{a}^*$ will be specified

later. Our main goal in this paper is to characterize the scaling-law and bottleneck behaviors of the excess risk

$$R(\mathbf{W}, \mathbf{a}) = \mathbb{E}_{\mathbf{x} \sim \mathcal{N}(0, \mathbf{I}_d)} [(f(\mathbf{x}; \mathbf{W}^*, \mathbf{a}^*) - f(\mathbf{x}; \mathbf{W}, \mathbf{a}))^2] \quad (3)$$

associated with the minimizers $\hat{\mathbf{W}}, \hat{\mathbf{a}}$ of eq. (1). We will consider two specific classes of shallow neural networks. Thanks to exact mappings to classical problems in signal processing, these models admit a mathematical characterization, enabling an end-to-end analysis of the non-convex optimization problem in the feature learning regime.

Diagonal networks and LASSO. The first architecture is a diagonal neural network with $p = d$, diagonal first-layer weights $\mathbf{W} = \text{diag}(\mathbf{w})$, linear activation and no bias ($\mathbf{b} = 0$):

$$f(\mathbf{x}; \mathbf{W}, \mathbf{a}) = \mathbf{a}^\top \frac{(\mathbf{w} \odot \mathbf{x})}{\sqrt{d}}. \quad (4)$$

While the expressivity of this architecture is the same as that of a linear model, the reparameterization creates an effective implicit regularization that allows for feature selection and has made this setting popular among theoreticians. Indeed, adapting an argument by Neyshabur et al. (2015); Soudry et al. (2018); Pesme & Flammarion (2023) (see Appendix A), the resulting empirical minimization problem is equivalent to the LASSO problem with parameters $\theta_i = a_i w_i / \sqrt{d}$ and objective

$$\hat{\boldsymbol{\theta}} = \arg \min_{\boldsymbol{\theta} \in \mathbb{R}^d} \frac{1}{2} \sum_{\mu=1}^n (y_\mu - \boldsymbol{\theta}^\top \mathbf{x}_\mu)^2 + \lambda \|\boldsymbol{\theta}\|_1. \quad (5)$$

In other words, the ERM problem for a diagonal two-layer linear network trained with ℓ_2 weight-decay can be understood through the performance of LASSO.

Quadratic neural network and matrix compressed sensing. The second architecture is that of an over-parameterized two-layer network with a (centered) quadratic activation,

$$f(\mathbf{x}; \mathbf{W}, \mathbf{a}) = \frac{1}{\sqrt{p}} \sum_{j=1}^p \left(\left(\frac{\mathbf{w}_j^\top \mathbf{x}}{\sqrt{d}} \right)^2 - \frac{\|\mathbf{w}_j\|_2^2}{d} \right) = \text{Tr} \left[\mathbf{S} \frac{\mathbf{x} \mathbf{x}^\top - \mathbf{I}_d}{\sqrt{d}} \right], \quad (6)$$

where $\mathbf{S} := \frac{\mathbf{W}^\top \mathbf{W}}{\sqrt{pd}} \in \mathbb{R}^{d \times d}$ and the normalization is taken for convenience. In this case, we fix the second-layer weight \mathbf{a} of the model to be an all-one vector, but the target network may have arbitrary second layer weights. This class of quadratic neural networks have recently gained in popularity as simple models for non-convex tasks (Sarao Mannelli et al., 2020; Arnaboldi et al., 2023; Martin et al., 2024; Ben Arous et al., 2025). The ERM problem in eq. (1) for this architecture can be mapped to a sparse estimation setting (Gunasekar et al., 2017; Maillard & Kunisky, 2024; Bandeira & Maillard, 2025; Xu et al., 2025; Erba et al., 2025), namely matrix compressed sensing (or low-rank matrix estimation):

$$\hat{\mathbf{S}} = \arg \min_{\mathbf{S} \succeq 0} \sum_{\mu=1}^n (y_\mu - \text{Tr}[\mathbf{S} \mathbf{Z}_\mu])^2 + \lambda \|\mathbf{S}\|_*, \quad (7)$$

where $\mathbf{Z}_\mu := \frac{\mathbf{x}_\mu \mathbf{x}_\mu^\top - \mathbf{I}_d}{\sqrt{d}}$ and $\|\cdot\|_*$ denotes the nuclear norm. We refer again to Appendix A for the explicit mapping. Thus, the performance of a quadratic network trained with weight decay can be analyzed via low-rank matrix estimation with nuclear norm regularization.

These two equivalences underline the central theme of this work: by mapping neural network training problems to sparse vector and matrix estimation tasks, we can leverage the rich theoretical toolbox developed for LASSO and compressed sensing, and in particular approximate message passing and its high-dimensional state evolution (Donoho et al., 2009; 2013; Javanmard & Montanari, 2013; Berthier et al., 2020; Erba et al., 2025). This bridge not only enables precise predictions for generalization error and scaling exponents, but also provides a principled understanding of the weight spectral distribution in neural networks.

Power-law/quasi-sparse targets. To study scaling behavior, we adopt the classical assumption of a target with a power-law spectrum, as considered for instance in (Caponnetto & De Vito, 2007;

108 Steinwart et al., 2009; Spigler et al., 2020; Cui et al., 2021; Bordelon et al., 2024; Ben Arous et al.,
 109 2025). In the language of compressed sensing, this corresponds to the notion of *quasi-sparsity*
 110 (Negahban & Wainwright, 2011; Raskutti et al., 2011), where the signal is not exactly sparse but
 111 its coefficients decay according to a heavy-tailed distribution. This makes the setting natural and
 112 relevant to both the machine learning and signal processing communities. Concretely, in the case of
 113 diagonal linear networks we assume effective weights

$$\theta_i^* \stackrel{i.i.d.}{\sim} \mathcal{N}(0, d i^{-2\gamma}), \quad \boldsymbol{\theta}^* := \mathbf{W}^* \mathbf{a}^*, \quad (8)$$

116 while for quadratic neural networks we assume that

$$S^* := \frac{1}{\sqrt{pd}} \sum_{j=1}^p a_j^* \mathbf{w}_j^* (\mathbf{w}_j^*)^T \quad (9)$$

120 is rotationally invariant with eigenvalues $\{\sqrt{d} i^{-\gamma}\}_{i=1}^d$. This setting was recently studied as well in
 121 Ben Arous et al. (2025) (who, however, considered noiseless target as opposed to our noisy eq. (2)
 122 and obtain one of our scaling exponents). In both cases we fix $\gamma > 1/2$ to ensure square-summability
 123 of $\boldsymbol{\theta}^*$ and S^* .
 124

125 1.1 MAIN RESULTS

127 **1. Phase diagram and complete characterization of excess risk rates for power-law targets.** We provide a sharp characterization of the excess risk achieved by empirical risk minimization (1)
 128 for both diagonal linear networks and quadratic networks in the regime $n, d \gg 1$ with $p \geq d$, under
 129 a power-law design for the target function and varying regularization strength λ , summarized in
 130 Figure 1. Our results uncover a striking universality between the two settings, including a transition
 131 from *benign* to *harmful overfitting*. Exploring the extent of this universality beyond the setting here
 132 is an interesting avenue for future work. We also derive the risk rates under optimal regularization
 133 λ , and show that optimally-regularized ERM achieves the Bayes-optimal rates — previously known
 134 only for the diagonal case (Raskutti et al., 2011). These findings are of independent interest for
 135 sparse vector and low-rank matrix estimation.

136 **2. Spectral behavior of the learned weights.** We characterize, across all phases, the spectral prop-
 137 erties of the trained network weights. The learned spectrum reflects the implicit trade-off between
 138 signal, noise, and regularization, and exhibits phenomena directly connected to feature learning.
 139 Remarkably, the resulting spectral behavior mirrors observations in modern deep learning practice
 140 (Martin & Mahoney, 2021a; Thamm et al., 2024).

141 **3. First-principles explanation of spectra-generalization connection.** We provide a clear inter-
 142 pretation of the spectrum and its relation to generalization. Building on Result 3, which decomposes
 143 the error into *underfitting*, *overfitting*, and *approximation* terms, we show that each of these com-
 144 ponents is directly connected to the spectral statistics of the weights. In doing so, we provide a
 145 mathematical theory for the empirical observations of Martin et al. (2021) and Wang et al. (2023)
 for the spectral statistics of weights in large-scale trained networks.

146 **4. Non-asymptotic validity of state evolution.** Our derivations rely on approximate message pass-
 147 ing (AMP) and its state evolution equations, which are rigorously valid only in the proportional
 148 asymptotic regime with fixed ratios n/d (or n/d^2) and fixed λ . We extend these equations heuristi-
 149 cally beyond their proven setting, covering arbitrary scalings of n, d, λ . Through extensive numeri-
 150 cal experiments, we demonstrate that state evolution remains accurate down to constants across the
 151 whole parameter space, including far beyond proven guarantees. This surprising robustness, already
 152 established in ridge regression (Cui et al., 2021; Cheng & Montanari, 2024; Misiakiewicz & Saeed,
 153 2024; Defilippis et al., 2024), suggests a broader conjecture: the AMP framework, and related tools
 154 from spin glass theory, may provide predictive power well outside their standard asymptotic as-
 155 sumptions. We hope this will further motivate work on non-asymptotic control of AMP (Rush &
 156 Venkataramanan, 2018; Miolane & Montanari, 2021; Li & Wei, 2022; Reeves, 2025).

157 Together, these results provide a comprehensive theoretical and empirical understanding of scaling
 158 laws for feature learning in simple network models.

159 1.2 FURTHER RELEVANT WORK

161 **Scaling laws —** A large body of work has studied scaling laws in the lazy regime, where the fea-
 162 tures remain fixed. This includes kernel methods (Caponnetto & De Vito, 2007; Spigler et al., 2020;

162 Cui et al., 2021), random features (Defilippis et al., 2024; Atanasov et al., 2024; Bahri et al., 2024;
 163 Maloney et al., 2022; Paquette et al., 2024; Kunstner & Bach, 2025), and neural tangent kernels
 164 (NTK) (Bordelon et al., 2020). Bordelon et al. (2024; 2025) analyzed how scaling laws change for
 165 linear networks when both weights are trained, and Worschach & Rosenow (2024) explicitly solves
 166 the dynamics of a linear network to obtain the scalings. Our goal in this work is to go beyond linear
 167 networks and the lazy regime and analyze scaling laws in the presence of genuine feature learning.
 168 Two recent works (Ren et al., 2025; Ben Arous et al., 2025) analyze settings related to ours, but with
 169 important differences. Both consider two-layer networks with sublinear width, orthogonal first-layer
 170 weights, and power-law decaying second-layer weights. Ren et al. (2025) study activation functions
 171 with large information exponents, which is orthogonal to our setting, while Ben Arous et al. (2025)
 172 focus on quadratic activations with a specific SGD dynamics. Both works, additionally, consider
 173 noiseless targets and unregularized training ($\lambda = \Delta = 0$). Here, instead, we study empirical risk
 174 minimization with weight decay in the noisy setting (which allows to observe benign and harmful
 175 overfitting).

176 **Spectral properties of learned weights** — A growing literature investigates the distribution of
 177 weight spectra in trained neural networks, with particular attention to the emergence of heavy-tailed
 178 eigenvalue distributions in both weights and activations (Mahoney & Martin, 2019; Martin et al.,
 179 2021; Martin & Mahoney, 2021b;a; Thamm et al., 2024; Wang et al., 2023; Zhou et al., 2023;
 180 Hodgkinson et al., 2025). Despite these empirical observations, a precise theoretical characterization
 181 of the learned spectra and their relation to generalization has remained elusive. Recent progress
 182 includes analyses of the spectrum after a single or a few gradient steps (Dandi et al., 2024; Moniri
 183 et al., 2023; Cui et al., 2024; Dandi et al., 2025; Kothapalli et al., 2025), as well as results showing
 184 convergence of SGD in mean-field models to spectral distributions reminiscent of those we obtain
 185 (Olsen et al., 2025). Our description of the spectrum of the trained weight provides an analytic
 186 characterization of this phenomenon, and provides an interpretation of these properties from first
 187 principles.

188 **AMP and State Evolution** — Our analysis relies on approximate message passing (AMP) and
 189 its state evolution (SE), which has become a central tool for studying high-dimensional inference
 190 problems with structure (Donoho et al., 2013; Bayati & Montanari, 2011; Javanmard & Montanari,
 191 2013; Berthier et al., 2020; Zou & Yang, 2022; Feng et al., 2022; Gerbelot & Berthier, 2023; Dudeja
 192 et al., 2023; Erba et al., 2025). It has also been applied to learning problems beyond sparse recovery,
 193 such as kernel methods and learning rates (Cui et al., 2021; Loureiro et al., 2021). In this work,
 194 we use the state evolution equations of AMP heuristically, to analyze quasi-sparse models *beyond*
 195 their rigorously proven asymptotic regimes (typically assuming a fixed ratio n/d). While recent
 196 advances in non-asymptotic control (Rush & Venkataraman, 2018; Miolane & Montanari, 2021;
 197 Li & Wei, 2022; Reeves, 2025) provide reassurance, a finer control of the limit is still required
 198 for a fully rigorous justification. Our experiments nevertheless show excellent agreement between
 199 SE predictions and numerical results across regimes, suggesting that AMP may be predictive well
 200 beyond its standard assumptions.

201 **Compressed sensing** — Quasi-sparse settings, where coefficients decay with a power law in
 202 Fourier or wavelet bases, have long been studied in statistics and signal processing. This is natural
 203 since most real-world signals are not exactly sparse but have heavy-tailed coefficient distributions
 204 (Mallat, 1999). Classical work on LASSO and matrix compressed sensing analyzed ℓ_p -controlled
 205 targets, deriving minimax bounds on error and sample complexity (Raskutti et al., 2011; Negahban
 206 & Wainwright, 2011). Our results extend this line of work by providing the full phase diagram
 207 across all regularization strengths and data scales. For instance, the optimal LASSO rate of Raskutti
 208 et al. (2011) arises from setting $\lambda = \tilde{\Theta}(\sqrt{n/d})$ (here $\tilde{\Theta}$ is up to logarithmic factors).

210 2 MAIN RESULTS

211 2.1 UNIVERSAL ERROR RATES

212 In this section we discuss the excess risk rates associated to the two problems introduced above. Our
 213 analysis is based on a deterministic characterization of the risk $\hat{R}(\hat{W}, \hat{a}) \simeq R_{n,d}$ at large $n, d \gg 1$,
 214 which is discussed in Section 2.4. In order to highlight the correspondence between the two neural

network models, we express the results in terms of the effective sample size n_{eff} as follows:

$$n_{\text{eff}} \equiv \begin{cases} n & \text{for diagonal network} \\ n/d & \text{for quadratic network} \end{cases} . \quad (10)$$

Surprisingly, this definition will be enough to present both cases in a unified manner.

Result 1 (Excess risk rates). *Under the setting of Sec. 1 for $\Delta > 0$ and $n_{\text{eff}} \gg 1$, the excess risk satisfies*

$$R_{n_{\text{eff}},d}(\lambda) = \begin{cases} \Theta\left(n_{\text{eff}}^{-1+1/(2\gamma)} + \rho(n_{\text{eff}}/d)\right) & \text{if } 1 \ll n_{\text{eff}} \ll d \text{ and } \lambda \ll \sqrt{\frac{n_{\text{eff}}}{d}} \\ \Theta(\lambda^{-2/3}) & \text{if } n_{\text{eff}} \sim d \text{ and } \lambda \ll 1 \\ \Theta(d/n_{\text{eff}}) & \text{if } n_{\text{eff}} \gg d \text{ and } \lambda \ll \sqrt{\frac{n_{\text{eff}}}{d}} \\ \Theta\left(\left(\lambda d^{1/2}/n_{\text{eff}}\right)^{2-1/\gamma}\right) & \text{if } \max\left(\sqrt{\frac{n_{\text{eff}}}{d}}, \frac{n_{\text{eff}}}{d^{1/2}}\right) \ll \lambda \ll \frac{n_{\text{eff}}}{d^{1/2}} \\ \Theta\left(\lambda^2 d^2/n_{\text{eff}}^2\right) & \text{if } \sqrt{\frac{n_{\text{eff}}}{d}} \ll \lambda \ll \frac{n_{\text{eff}}}{d^{1/2}} \end{cases} , \quad (11)$$

and $R_{n_{\text{eff}},d} = \Theta(1)$ otherwise, where $\rho(t) = -1/\log(t)$ in the diagonal network case and $\rho(t) = t^{2/5}$ in the quadratic network case. Notice that in both cases the ρ term is monotone increasing with n_{eff}/d , and dominates the error rate when $n_{\text{eff}} \rightarrow d$. Additionally, in the diagonal network case, the first rate holds up to logarithmic factors that we specify in eq. (91) in Appendix B.4.

These rates are summarized in Figure 1. For small (fixed) regularization $\lambda < 1/\sqrt{d}$, with d fixed and n_{eff} increasing, the excess error moves from an initial plateau (Phase Ia), driven by data scarcity, to a fast-decay (Phase IV), where $R_{n_{\text{eff}},d} = \Theta(n_{\text{eff}}^{-1+1/(2\gamma)})$, matching the minimax rate in (Raskutti et al., 2011; Donoho et al., 2011). As n_{eff} approaches d , the estimator begins to fit the noise, and we observe a harmful overfitting (Phase V), in which the excess risk is dominated by the non-universal scale ρ (arising from overfitting the noise as in Result 3). This transition, characteristic of the under-regularized and under-sampled regime ($1 \ll n_{\text{eff}} \ll d$, $\lambda \ll \sqrt{\frac{n_{\text{eff}}}{d}}$), happens at

$$n_{\text{eff}}^{\text{cross}} = \begin{cases} (\log d)^{\frac{4\gamma-1}{2\gamma-1}} & \text{for diagonal network} \\ d^{\frac{4\gamma}{14\gamma-5}} & \text{for quadratic network} \end{cases} . \quad (12)$$

The excess risk reaches its maximum around $n_{\text{eff}} \sim d$ with $R_{n_{\text{eff}},d} \sim \lambda^{-2/3}$. This non-monotonicity of the risk at interpolation is reminiscent of the double descent behavior (Belkin et al., 2019; Mei & Montanari, 2022), and extends previous findings (Bartlett et al., 2020; Wang et al., 2024) to non-linear models. For $n_{\text{eff}} \gg d$, the excess risk then enters a second fast-decay Phase VIa, with rate proportional to d/n_{eff} ; this is the fastest decay we observe, provided $n_{\text{eff}} \gg d^{2\gamma}$ (Phase VIb). For larger regularization strength $\lambda > 1/\sqrt{d}$, the excess risk decay is described by the upper part of the phase diagram in Figure 1, eventually crossing to the lower part when $n_{\text{eff}} \sim d\lambda^2$. In particular, if $\lambda \gg d^{1/2}$, we observe that increasing n_{eff} , the excess risk is initially in a plateau (Phase Ib), induced by the strong regularization with respect to the sample size. For $n \sim \lambda d^{1/2}$, it crosses into a slow rate Phase II with $R_{n_{\text{eff}},d} = \Theta(\lambda d^{1/2}/n_{\text{eff}})^{2-1/\gamma}$, which transitions to a faster rate (Phase III), still influenced by the large regularization, for $n_{\text{eff}} \sim \lambda d^{\gamma+1/2}$, with $R_{n_{\text{eff}},d} = \Theta((\lambda d/n_{\text{eff}})^2)$. Phase II recovers the rate in (Negahban & Wainwright, 2011, Corollary 2). The excess risk eventually transitions to the fast-decay Phase VIb for $n_{\text{eff}} \sim \lambda^2 d$, where the effect of the regularization becomes negligible due to the large sample size. These cross-overs are reminiscent of the ones observed for kernel and random feature ridge regression respectively in Cui et al. (2021); Defilippis et al. (2024).

We observe that there are region boundaries along which the rates are discontinuous (red lines in Figure 1). At the boundary $n_{\text{eff}} = \Theta(d)$, we observe the aforementioned crossover between harmful overfitting and fast decay, with an interpolation peak emerging. At the boundary $d \ll n_{\text{eff}} \ll d^{2\gamma}$ and $\lambda = \Theta(\sqrt{n_{\text{eff}}/d})$, the excess risk jumps from d/n_{eff} to $n_{\text{eff}}^{-1+1/(2\gamma)}$ (which is much lower) when increasing the regularization.

As a corollary of the above results, we can immediately estimate the behavior of the optimal regularization λ_{opt} and the associated optimal ERM rates.

Corollary 1 (Optimal regularization and optimality of ERM). *The optimal regularization satisfies*

$$\lambda_{\text{opt}}(n_{\text{eff}}, d) = \begin{cases} O(\sqrt{n_{\text{eff}}/d}), & \text{if } \Delta > 0 \text{ and } (1 \ll n_{\text{eff}} \ll n_{\text{eff}}^{\text{cross}} \text{ or } n_{\text{eff}} \gg d^{2\gamma}) \\ \tilde{\Theta}(\sqrt{n_{\text{eff}}/d}), & \text{if } \Delta > 0 \text{ and } n_{\text{eff}}^{\text{cross}} \ll n_{\text{eff}} \ll d^{2\gamma} \end{cases} . \quad (13)$$

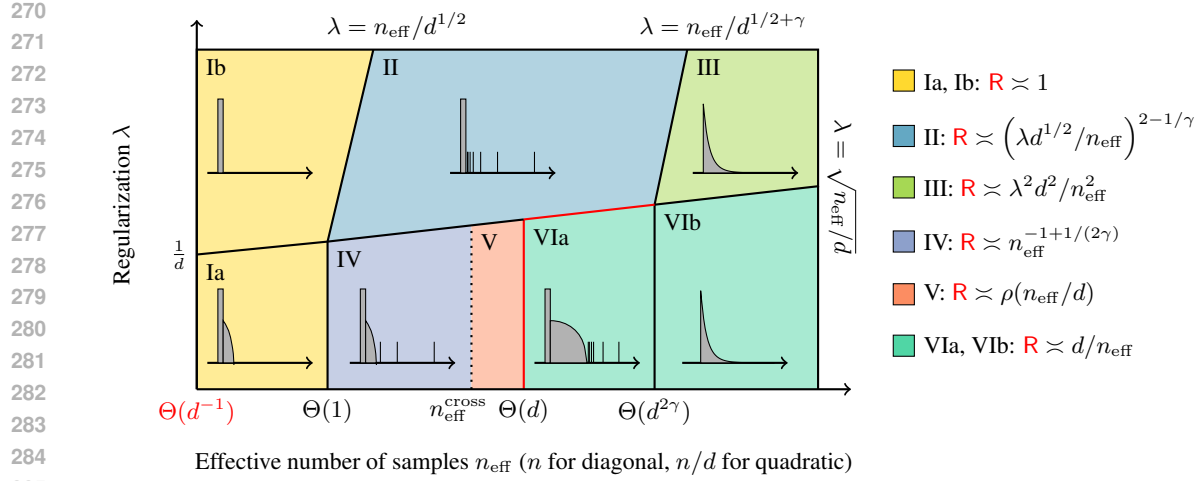


Figure 1: Excess risk rates of Result 1 as a function of n and $\lambda(n, d)$, with a sketch of the corresponding spectral properties of the learned weights (Result 2). Red lines represent discontinuous phase boundaries.

where $\tilde{\Theta}$ is up to logarithm factors in the argument. The excess risk rates in the optimally regularized case matches the large $n_{\text{eff}}, d \gg 1$ Bayesian risk $R_{\text{BO}}(\mathcal{D}) = \mathbb{E}[R(\mathbf{W}, \mathbf{a})|\mathcal{D}] \simeq R_{n_{\text{eff}}, d}^{\text{BO}}$ ¹ (for the diagonal network, up to logarithmic factors), given by

$$R_{n_{\text{eff}}, d}(\lambda_{\text{opt}}) = \Theta(R_{n_{\text{eff}}}^{\text{BO}}) = \begin{cases} \Theta(n_{\text{eff}}^{-1+1/(2\gamma)}) & \text{if } \Delta > 0 \text{ and } 1 \ll n_{\text{eff}} \ll d^{2\gamma} \\ \Theta(d/n_{\text{eff}}) & \text{if } \Delta > 0 \text{ and } n_{\text{eff}} \gg d^{2\gamma} \end{cases}, \quad (14)$$

and $R_{n_{\text{eff}}, d} = \Theta(1)$ otherwise. Again, in the diagonal network case, in the first regime the rate holds up to logarithmic factors that we specify in eq. (91) in Appendix B.4.

Corollary 1 shows that by appropriately tuning the regularization allows to avoid the harmful overfitting phase in the noisy case and reach Bayesian optimality. Interestingly, the noisy rate $\Theta(n_{\text{eff}}^{-1+1/(2\gamma)})$ in the regime $1 \ll n_{\text{eff}} \ll d^{2\gamma}$ coincides with the classical minimax rate for high-dimensional linear regression over an ℓ_q -ball with $q = 1/\gamma$ (Raskutti et al., 2011; Donoho et al., 2011). Corollary 1 not only recovers the well-known result that properly regularized LASSO achieves this minimax rate, but also extends it to additional regimes and to the matrix case, revealing a cross-over between the minimax rate and a faster $\Theta(d/n_{\text{eff}})$ rate.

2.2 SPECTRA OF THE LEARNED WEIGHTS

Our second set of results concerns the structural properties of the learned weights, that are given by a soft thresholding function applied to a noisy version of the target's weights. Notice that for diagonal neural networks, the weights θ can be seen as a diagonal matrix (modulo a sign), hence they coincide with the eigenvalues of \mathbf{W} .

Result 2 (Spectrum of the learned weights). *For the diagonal network case, there exists constants $\delta(n, d, \lambda)$ and $\epsilon(n, d, \lambda)$ (specified in Appendix B.1.2) such that the empirical risk estimator (1) satisfies (in distribution)*

$$\hat{\theta}_i \sim \sigma_d(\theta_i^* + \delta z_i; \epsilon), \quad (15)$$

where $z_i \sim \mathcal{N}(0, 1)$, and $\sigma_d(x; a) = \max(x - a, 0) - \max(-x - a, 0)$ is the soft-thresholding function. For the quadratic network case, there exists constants $\delta(n, d, \lambda)$ and $\epsilon(n, d, \lambda)$ (that are obtained from (20)) such that the spectrum ν of the empirical risk estimator (7) satisfies

$$\nu(x) = F_{\mu_\delta}(\lambda\epsilon)\delta_0(x) + \mu_\delta(x + \lambda\epsilon)\mathbf{1}_{x>0}. \quad (16)$$

δ_0 represents a Dirac mass at 0, $\mathbf{1}_A$ is the indicator function of the set A and μ_δ represents the spectrum of $\mathbf{S}^* + \delta \mathbf{Z}$ with its cumulative function F_{μ_δ} , where $\mathbf{Z} \sim \text{GOE}(d)$ (i.e. a symmetric matrix with $\mathcal{N}(0, 1/d)$ elements up to symmetry).

¹See section 2.4 for a formal statement.

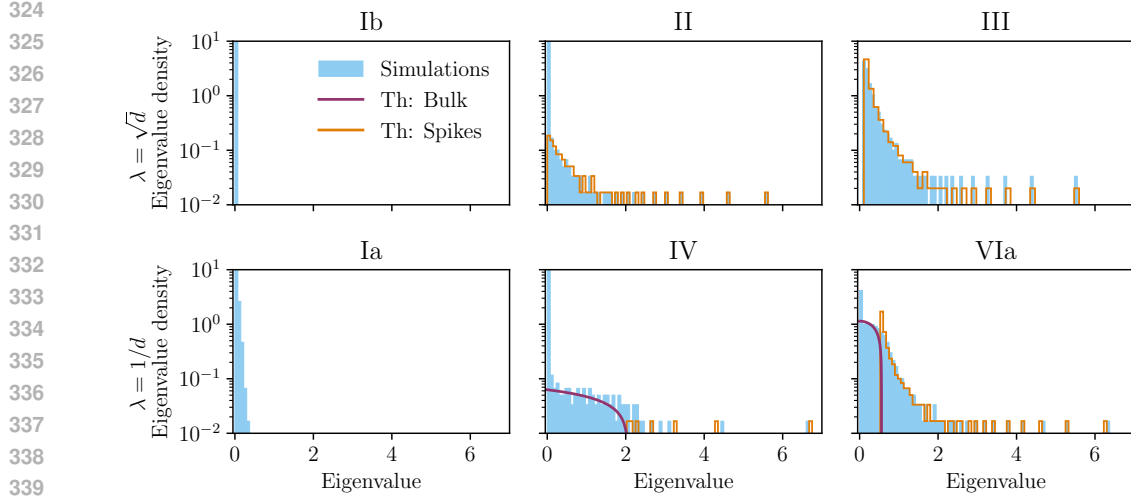


Figure 2: Comparison between spectra from simulations and theory across different training phases. Blue: eigenvalue histograms after training. Purple/orange: theoretical predictions for bulk and spikes, respectively (16) (for clarity, spike histograms are shown separately). Notice that our theory also predicts a spike at zero, which we do not plot for visual clarity. All panels use $d = 800$ except III, for which we have $d = 400$. Bottom row: $\lambda = 1/d$ with $n = 100, 1.94 \times 10^4, 1.28 \times 10^6$. Top row: $\lambda = \sqrt{d}$ with $n = 800, 6.4 \times 10^6, 2 \times 10^7$. We discuss the phenomenology in Section 2.3.

Result 2 characterizes the learned weights in both settings: they are *noisy, soft-thresholded versions of the target spectrum*. The parameter δ quantifies the noise from the label noise and finite sample estimation of the target weights, while $\lambda\epsilon$ sets the cutoff below which singular values vanish due to regularization. For any n, d, λ , the spectrum consists of a spike at zero, possibly a bulk near zero, and a few outliers aligned with the top eigenvectors of the target.

2.3 INTERPRETABILITY, AND A “UNIVERSAL” ERROR DECOMPOSITION

The spectra depends on n, d, λ only through the functions δ, ϵ , leading to a qualitative structure shared by both models. Our theory predicts eight distinct spectral phases (Figure 1) which are closely connected to the risk rates in Result 1. Focusing now on the quadratic network, the result provides an interpretation of the risk in terms of the weights spectrum.

Result 3 (“Universal” error decomposition of feature learning). *Let $\{s_i\}_{i=1}^d$ be the eigenvalues of S^* in non-increasing order. Consider the following two cases.*

(i): *Under-regularization. Assume that the constants $\delta(n, d, \lambda)$ and $\epsilon(n, d, \lambda)$ in Result 2 satisfy $\lambda\epsilon < 2\delta$ and there exists a cutoff $K(\delta) \ll d$ satisfying $s_{K(\delta)} = \delta$. Then the excess risk reads*

$$\begin{aligned}
 R_{n,d} = & \underbrace{\delta^2 \int_{\lambda\epsilon/\delta}^2 \mu_{\text{sc}}(dx) \left(x - \frac{\lambda\epsilon}{\delta} \right)^2 + \frac{1}{d} \delta K'(\delta) (2\delta - \lambda\epsilon)^2}_{\text{overfitting} \atop \text{(learned noise)}} \\
 & + \underbrace{\frac{1}{d} \sum_{i=K(\delta)+1}^d s_i^2}_{\text{underfitting} \atop \text{(not learned features)}} + \underbrace{\frac{1}{d} \sum_{i=1}^{K(\delta)} \left[\left(\frac{\delta^2}{s_i} - \lambda\epsilon \right)^2 + \frac{\delta^2}{s_i} \left(s_i + \frac{\delta^2}{s_i} - \lambda\epsilon \right) \right]}_{\text{approximation error} \atop \text{for learned features}}.
 \end{aligned} \tag{17}$$

where $\mu_{\text{sc}}(dx) = (2\pi)^{-1} \sqrt{4 - x^2} \mathbf{1}_{x \in [-2, 2]} dx$ denotes the Wigner semi-circle law.

(ii): *Over-regularization. Assume that the constants $\delta(n, d, \lambda)$ and $\epsilon(n, d, \lambda)$ in Result 2 satisfy $\lambda\epsilon \geq 2\delta$ and there exists a cutoff $K(\delta, \lambda\epsilon) \ll d$ satisfying $s_{K(\delta, \lambda\epsilon)} + \frac{\delta^2}{s_{K(\delta, \lambda\epsilon)}} - \lambda\epsilon = 0$. Then the*

378 *excess risk reads*

$$379 \quad R_{n,d} = \underbrace{\frac{1}{d} \sum_{i=K(\delta, \lambda\epsilon)+1}^d s_i^2}_{\text{underfitting} \atop \text{(not learned features)}} + \underbrace{\frac{1}{d} \sum_{i=1}^{K(\delta, \lambda\epsilon)} \left[\left(\frac{\delta^2}{s_i} - \lambda\epsilon \right)^2 + \frac{\delta^2}{s_i} \left(s_i + \frac{\delta^2}{s_i} - \lambda\epsilon \right) \right]}_{\text{approximation error} \atop \text{for learned features}}. \quad (18)$$

380
381
382
383
384

385 Equations (17) and (18) have clear interpretations. The first component of the overfitting term corre-
386 sponds to the second moment of the bulk spectrum, representing the power of the learned noise and
387 thus quantifying the degree of overfitting. The second part of the overfitting term is proportional to
388 the square of the bulk size, but always remains subdominant compared to the first term. As shown
389 in Equation (18), the overfitting term diminishes with increasing regularization strength.

390 The underfitting term measures the mean power of the unlearned spikes, indicating how many fea-
391 tures are lost due to the cutoff $K(\delta, \lambda\epsilon)$ (which depends on the noise and regularization). The
392 approximation error term reflects the average error in the learned spikes, which depends on the ef-
393 fective signal-to-noise ratio $\frac{s_i}{\delta}$ and the effective regularization $\lambda\epsilon$. Notably, when the effective noise
394 δ is zero, the approximation error increases with regularization; conversely, when the regularization
395 λ is zero, the approximation error increases with noise $\frac{\delta}{s_i}$. In general, however, the approximation
396 error arises from a non-trivial interplay between the effective noise and regularization.

397 This decomposition is “universal” in that it does not depend on the target spectrum, dataset size, or
398 regularization, holds for all $\Delta \geq 0$ and applies across different spectral phases. While derived here
399 for quadratic networks, similar expressions hold as well for diagonal networks. See Appendix B.1.2.
400 Extending it to broader architectures is an interesting direction for future work.

401 Based on the error decomposition in Result 3, we give an interpretation of the rates in Result 1 in
402 terms of the weight spectral properties (see Figure 1 for illustrations and Figure 2 for experiments):
403 the bulk corresponds to learned noise, the spikes hidden by the bulk are the unlearned features, and
404 the outliers are the learned features. This provides a mathematical theory from first principles for the
405 observations of (Martin & Mahoney, 2021a; Martin et al., 2021), whose terminology (e.g. “bleed-
406 out”, “rank collapse”, . . .) we borrow in the following. We begin by the case of large regularization,
407 considering an increasing number of samples.

- 408 • **Ib (Rank collapse):** All eigenvalues are zero. Data scarcity and strong regularization imply that
409 the ERM estimator is zero. Result 3 then gives a trivial risk $R = \text{Tr}[(S^*)^2]/d$.
- 410 • **II (Outliers):** The spectrum contains approximately $N_{\text{out}} = (\frac{4n}{\lambda d^{3/2}})^{1/\gamma}$ outliers, while the
411 remaining eigenvalues are zero. Spikes are shifted by $\approx \frac{\lambda d^2}{4n}$. In this regime, some features are
412 learned with noise, while others are lost due to over-regularization. Result 3 implies that the risk
413 is determined by the number and shift of the spikes, yielding $R = \Theta\left(\frac{1}{d} \sum_{i \geq N_{\text{out}}} (\sqrt{d}i^{-\gamma})^2\right) =$
414 $\Theta\left((\lambda d^{3/2}/n)^{2-1/\gamma}\right)$, since the error from the shift is of the same order.
- 415 • **III (Heavy-tail):** The spectrum is a perturbed version of the target spectrum with a heavy-tail
416 $\rho(x) \sim x^{-1-1/\gamma}$. Regularization shifts the bulk leftward by $\approx \frac{\lambda d^2}{4n}$, yielding $R = \Theta\left((\lambda d^2/n)^2\right)$.

417 As more eigenvalues emerge from the spike at zero, more features are learned and the risk decreases.
418 Strong regularization suppresses any spurious bulk of small eigenvalues, as well as some of the
419 smaller spikes. Consider now the case of small regularization.

- 420 • **Ia (Rank collapse):** The spectrum resembles a small portion of a semi-circle law along with many
421 zero eigenvalues. Perhaps surprisingly, the contribution of the bulk is negligible even for vanishing
422 regularization. Neither features nor noise are learned, so the risk remains $R = \text{Tr}[(S^*)^2]/d$.
- 423 • **IV (Bulk + Outliers):** The spectrum exhibits $N_{\text{out}} = (\Delta d/4n)^{-1/2\gamma}$ outliers and a bulk with
424 eigenvalues of order $\Theta((\Delta^5 d^2/n)^{1/10})$. As in Phase II, the risk decreases as more spikes emerge
425 from the bulk. Since the bulk contribution is sub-leading, Result 3 implies that the risk scales as
426 the average power of the unlearned spikes: $R = \frac{1}{d} \sum_{i \geq N_{\text{out}}} (\sqrt{d}i^{-\gamma})^2 = \Theta\left((d/n)^{1-\frac{1}{2\gamma}}\right)$.
- 427 • **V (Bulk + Outliers):** Similar to Phase IV, but the risk is now dominated by the bulk of eigenvalues
428 of order $\Theta((\Delta^5 d^2/n)^{1/10})$. The ERM estimator approaches interpolation and begins to fit noise.

432 Although the number of outliers ($N_{\text{out}} = \Delta d/4n$) $^{-1/2\gamma}$ continues to increase and the bulk range
 433 shrinks, the bulk's second moment grows. Altogether, Result 3 implies the risk increases.
 434

- 435 • **Interpolation peak (Bulk + Outliers):** The spectrum is dominated by a large semi-circle bulk
 436 of order $\Theta(\Delta^{2/3}\lambda^{-1/3})$. There may still be $\Theta(\Delta^{2/3}\lambda^{-1/3}d^{-1/2})$ spikes if $\lambda \gg d^{-3/2}$, but their
 437 contribution is negligible. Even if the model learns features, the noise is overwhelming, and
 438 Result 3 implies the risk is dominated by the bulk second moment $R = \Theta(\lambda^{-2/3})$.
- 439 • **VIa (Bulk + Bleed-out + Outliers):** The spectrum contains $(\Delta d/4n)^{-1/2\gamma}$ outliers and a bulk of
 440 small eigenvalues of order $\sqrt{\Delta d^2/4n}$. The smallest outliers merge at the bulk boundary, creating
 441 a *bleed-out* effect. The risk decreases as more outliers emerge. The spikes are perturbed by
 442 $\Theta(\sqrt{\Delta d^2/n})$, and Result 3 implies the risk scales as $R = \Theta(d^2/n)$, since this dominates over the
 443 unlearned features.
- 444 • **VIb (Heavy-tail):** As in Phase III, the spectrum is a perturbed version of the target (a *heavy-tailed*
 445 bulk) with perturbations of order $\Theta(\sqrt{\Delta d^2/n})$. The risk decays with the perturbation strength as
 446 $R = \Theta(d^2/n)$.
 447

448 Therefore, for the under-regularized case, as the number of samples is increased, the bulk keeps
 449 shrinking as the spikes pop out. However, as the shape of the bulk and the number of zero eigen-
 450 values changes, the risk changes non-monotonically. In other words, the model learns an increasing
 451 number of features, but the influence of noise leads to a non-monotonic behavior in the risk. Fur-
 452 thermore, Result 3 shows that regularization only affects the first term of eq. (17) and may increase
 453 the last two terms. Thus the optimal regularization strategy is to truncate the bulk, setting the first
 454 term to zero, leaving the second unchanged and minimally increasing the third. If the bulk contribu-
 455 tion is negligible, weaker regularization may be chosen (i.e. in phases IV and VIb). This reasoning
 456 explains Corollary 1.

457 Finally, we should note that although phases VIa and VIb exhibit similar risk decay rates, only
 458 VIb achieves the Bayes-optimal rate. In the regime $d \ll n_{\text{eff}} \ll d^2$, the optimal performance is
 459 reached in phase II with $\lambda = \sqrt{n_{\text{eff}}/d}$. The corresponding spectral density shows a transition from
 460 outlier-dominated (zero eigenvalues+spikes) to heavy-tailed behavior, which supports the argument
 461 of Martin et al. (2021) that heavy-tailed spectra are associated with superior generalization.

462 2.4 NON-ASYMPTOTIC STATE EVOLUTION

463 The results of Sections 2.1, 2.2 and 2.3 build on the theory of state evolution and approximate mes-
 464 sage passing algorithms (Donoho et al., 2009; Javanmard & Montanari, 2013; Gerbelot & Berthier,
 465 2023), whose formal guarantees hold in the high-dimensional limit $n_{\text{eff}}, d \rightarrow \infty$ with fixed ratio
 466 n_{eff}/d and constant strength λ . In this regime, state evolution allows to characterize the asymptotic
 467 risk and the spectrum of the weights in both the neural networks models under consideration, both
 468 for the empirical risk minimizer and for the Bayes-optimal estimator (see Appendices B and C).

469 Non-rigorous analyses in the ridge regression literature have employed asymptotic formulas to
 470 estimate excess risk rates under source & capacity conditions, recovering classical results while also
 471 identifying new regimes in striking agreement with finite-size numerical experiments (Bordelon
 472 et al., 2020; Cui et al., 2021; Simon et al., 2023). The validity of these formulas beyond proportional
 473 asymptotics was subsequently established through non-asymptotic multiplicative bounds, thereby
 474 placing these rates on rigorous grounds (Cheng & Montanari, 2024; Misiakiewicz & Saeed, 2024;
 475 Defilippis et al., 2024). Motivated by this line of work, we derive our results under an analogous
 476 assumption: namely, that the state evolution equations for LASSO and matrix compressed sensing
 477 remain valid beyond proportional asymptotics. This assumption is supported both by extensive
 478 numerical evidence, depicted in Figure 3 and Appendices B, E, and by rigorous results on the con-
 479 vergence rates for the LASSO state evolution (Miolane & Montanari, 2021)². Figure 3 also confirms
 480 the theoretical decay rates of the excess risk across all phases, with state evolution and simulations
 481 in excellent agreement (see Appendix E for details on the implementation). Nonetheless, estab-
 482 lishing non-asymptotic multiplicative bounds for LASSO and matrix compressed sensing remains
 483 a challenging open problem. Our results provide both motivation and supporting evidence for this
 484 direction, which we leave for future work. For conciseness, we only present the conjecture regarding
 485 quadratic networks, and refer to Appendix B for the conjecture concerning diagonal networks.

²However, we need to extend their results to finite sample analysis (Rush & Venkataraman, 2018)

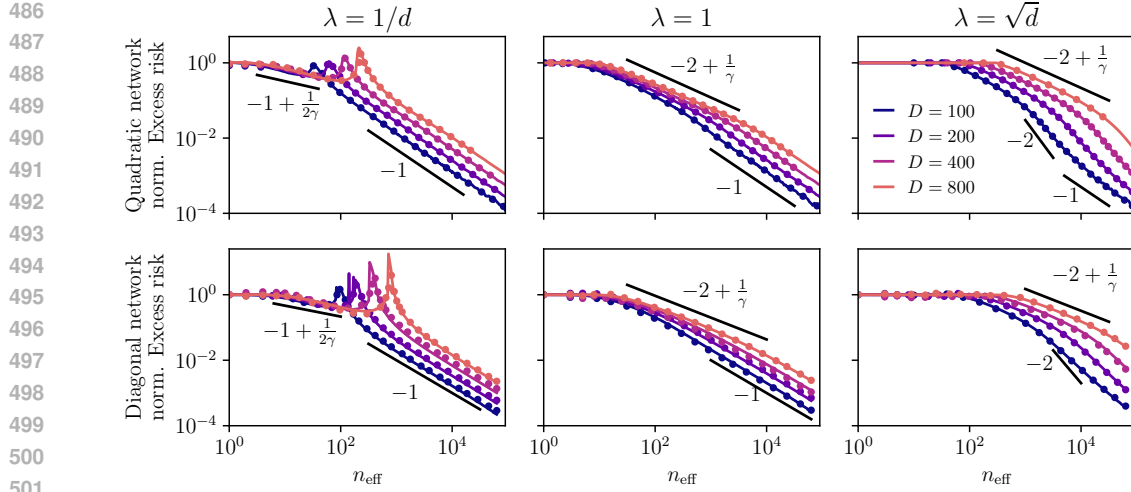


Figure 3: Excess risk in simulations (dots, $d = 100, 200, 400, 800$) versus non-asymptotic state evolution (solid lines) as a function of n_{eff} ($n_{\text{eff}} = n$ for the diagonal case, $n_{\text{eff}} = n/d$ for the quadratic case) with $\lambda = 1/d, 1, \sqrt{d}$ and $\Delta = 0.5$. We find excellent agreement, despite state evolution being rigorous only in the asymptotic limit $n_{\text{eff}}/d = \Theta(1)$ with $d \gg 1$. Black lines indicate the decay rates of the excess risk predicted by Result 1, again showing good agreement.

Conjecture 1. Let $\lambda > 0$, $\Delta \geq 0$ and consider $n, d \gg 1$ sufficiently large. Then with a probability at least $1 - o_n(1) - o_d(1)$, both the excess risk associated to the empirical risk minimizer eq. (7) and the Bayes-optimal risk (i.e. either R_{BO} or $R(\hat{\mathbf{W}}, \hat{\mathbf{a}})$) satisfy $|R - R_{n,d}| = R_{n,d} \cdot o_{n,d}(1)$. More precisely, for the Bayes-optimal case we have $R_{n,d}^{\text{BO}} = \frac{1}{d} \text{Tr}[(\mathbf{S}^*)^2] - q$ with q given by the fixed point of the following equation

$$\hat{q} = \frac{4n/d^2}{\Delta + 2(Q^* - q)}, \quad 1 - 2\tilde{\alpha} + \frac{\Delta\hat{q}}{2} = \frac{4\pi^2}{3\hat{q}} \int \mu_{1/\sqrt{\hat{q}}}(x)^3 dx, \quad (19)$$

where $\mu_{1/\sqrt{\hat{q}}}$ denotes the spectrum of $\mathbf{S}^* + \frac{1}{\sqrt{\hat{q}}}\mathbf{Z}$ with $\mathbf{Z} \sim \text{GOE}(d)$. For the ERM, $R_{n,d} = \frac{2n}{d^2}\delta^2 - \frac{\Delta}{2}$, where δ is given by the fixed point of the following equation

$$\begin{cases} 4\frac{n}{d^2}\delta - \frac{\delta}{\epsilon} = \partial_1 J(\delta, \lambda\epsilon), \\ Q^* + \frac{\Delta}{2} + 2\frac{n}{d^2}\delta^2 - \frac{\delta^2}{\epsilon} = (1 - \lambda\epsilon\partial_2)J(\delta, \lambda\epsilon), \end{cases} \quad J(a, b) := \int_b^{+\infty} \mu_a(x)(x - b)^2 dx. \quad (20)$$

with μ_a denoting the spectrum of $\mathbf{S}^* + a\mathbf{Z}$ with $\mathbf{Z} \sim \text{GOE}(d)$.

3 CONCLUSION

We studied a theoretical framework for scaling laws in shallow networks with feature learning by mapping them to sparse vector and low-rank matrix estimation. This allowed us to derive a comprehensive phase diagram for the excess risk scaling laws, uncovering a universality between diagonal and quadratic networks. Our analysis provides a first-principles explanation of the weight spectra–generalization connection: underfitting, overfitting, and approximation errors correspond directly to distinct spectral features, yielding a firm foundation for empirical observations of heavy-tailed weight spectra and their link to generalization.

There are many natural extensions of this work, such as exploring additional structures present in the data (e.g., non-trivial covariances (Wortsman & Loureiro, 2025)), extending beyond two-layer networks and quadratic activations (Barbier et al., 2025), providing a rigorous proof of the state evolution conjecture following Miolane & Montanari (2021). Moreover, our current work only analyzes the global minimum, so we should also look at compute scaling laws of GD/SGD (Ben Arous et al., 2025) as well as the implicit biases of SGD towards heavy tails and its relation to generalization (Gurbuzbalaban et al., 2021; Simsekli et al., 2020; Hodgkinson et al., 2022). We hope these results will motivate further progress toward a systematic theory of neural scaling laws.

540 REFERENCES
541

542 Luca Arnaboldi, Florent Krzakala, Bruno Loureiro, and Ludovic Stephan. Escaping mediocrity:
543 how two-layer networks learn hard generalized linear models with SGD. *arXiv preprint*
544 *arXiv:2305.18502*, 2023.

545 Alexander Atanasov, Jacob A Zavatone-Veth, and Cengiz Pehlevan. Scaling and renormalization in
546 high-dimensional regression. *arXiv preprint arXiv:2405.00592*, 2024.

547 Yasaman Bahri, Ethan Dyer, Jared Kaplan, Jaehoon Lee, and Utkarsh Sharma. Explaining neural
548 scaling laws. *Proceedings of the National Academy of Sciences*, 121(27):e2311878121, 2024.

549 Afonso S Bandeira and Antoine Maillard. Exact threshold for approximate ellipsoid fitting of ran-
550 dom points. *Electronic Journal of Probability*, 30:1–46, 2025.

551 Jean Barbier, Francesco Camilli, Minh-Toan Nguyen, Mauro Pastore, and Rudy Skerk. Statistical
552 physics of deep learning: Optimal learning of a multi-layer perceptron near interpolation. *arXiv*
553 *preprint arXiv:2510.24616*, 2025.

554 Peter L Bartlett, Philip M Long, Gábor Lugosi, and Alexander Tsigler. Benign overfitting in linear
555 regression. *Proceedings of the National Academy of Sciences*, 117(48):30063–30070, 2020.

556 Mohsen Bayati and Andrea Montanari. The dynamics of message passing on dense graphs, with
557 applications to compressed sensing. *IEEE Transactions on Information Theory*, 57(2):764–785,
558 2011.

559 Mikhail Belkin, Daniel Hsu, Siyuan Ma, and Soumik Mandal. Reconciling modern machine-
560 learning practice and the classical bias–variance trade-off. *Proceedings of the National Academy*
561 *of Sciences*, 116(32):15849–15854, 2019.

562 Gérard Ben Arous, Murat A Erdogdu, N Mert Vural, and Denny Wu. Learning quadratic neural
563 networks in high dimensions: SGD dynamics and scaling laws. *arXiv preprint arXiv:2508.03688*,
564 2025.

565 Raphael Berthier, Andrea Montanari, and Phan-Minh Nguyen. State evolution for approximate
566 message passing with non-separable functions. *Information and Inference: A Journal of the IMA*,
567 9(1):33–79, 2020.

568 Blake Bordelon, Abdulkadir Canatar, and Cengiz Pehlevan. Spectrum dependent learning curves in
569 kernel regression and wide neural networks. In *International Conference on Machine Learning*,
570 pp. 1024–1034. PMLR, 2020.

571 Blake Bordelon, Alexander Atanasov, and Cengiz Pehlevan. A dynamical model of neural scaling
572 laws. *Proceedings of the 41st International Conference on Machine Learning*, 2024. arXiv
573 preprint arXiv:2402.01092.

574 Blake Bordelon, Alexander Atanasov, and Cengiz Pehlevan. How feature learning can improve
575 neural scaling laws. *Journal of Statistical Mechanics: Theory and Experiment*, 2025(8):084002,
576 2025.

577 Tom Brown, Benjamin Mann, Nick Ryder, Melanie Subbiah, Jared D Kaplan, Prafulla Dhariwal,
578 Arvind Neelakantan, Pranav Shyam, Girish Sastry, Amanda Askell, et al. Language models are
579 few-shot learners. *Advances in neural information processing systems*, 33:1877–1901, 2020.

580 Andrea Caponnetto and Ernesto De Vito. Optimal rates for the regularized least-squares algorithm.
581 *Foundations of Computational Mathematics*, 7(3):331–368, 2007.

582 Chen Cheng and Andrea Montanari. Dimension free ridge regression. *The Annals of Statistics*, 52
583 (6):2879–2912, 2024.

584 Hugo Cui, Bruno Loureiro, Florent Krzakala, and Lenka Zdeborová. Generalization error rates
585 in kernel regression: The crossover from the noiseless to noisy regime. *Advances in Neural*
586 *Information Processing Systems*, 34:10131–10143, 2021.

594 Hugo Cui, Luca Pesce, Yatin Dandi, Florent Krzakala, Yue Lu, Lenka Zdeborov, and Bruno
 595 Loureiro. Asymptotics of feature learning in two-layer networks after one gradient-step. In
 596 Ruslan Salakhutdinov, Zico Kolter, Katherine Heller, Adrian Weller, Nuria Oliver, Jonathan Scar-
 597 lett, and Felix Berkenkamp (eds.), *Proceedings of the 41st International Conference on Machine
 598 Learning*, volume 235 of *Proceedings of Machine Learning Research*, pp. 9662–9695. PMLR,
 599 21–27 Jul 2024.

600 Yatin Dandi, Florent Krzakala, Bruno Loureiro, Luca Pesce, and Ludovic Stephan. How two-layer
 601 neural networks learn, one (giant) step at a time. *Journal of Machine Learning Research*, 25(349):
 602 1–65, 2024.

603 Yatin Dandi, Luca Pesce, Hugo Cui, Florent Krzakala, Yue Lu, and Bruno Loureiro. A random
 604 matrix theory perspective on the spectrum of learned features and asymptotic generalization ca-
 605 pabilities. In Yingzhen Li, Stephan Mandt, Shipra Agrawal, and Emtiyaz Khan (eds.), *Proceed-
 606 ings of The 28th International Conference on Artificial Intelligence and Statistics*, volume 258 of
 607 *Proceedings of Machine Learning Research*, pp. 2224–2232. PMLR, 03–05 May 2025.

608 Leonardo Defilippis, Bruno Loureiro, and Theodor Misiakiewicz. Dimension-free deterministic
 609 equivalents and scaling laws for random feature regression. *Advances in Neural Information
 610 Processing Systems*, 37:104630–104693, 2024.

611 David Donoho, Iain Johnstone, Arian Maleki, and Andrea Montanari. Compressed sensing over
 612 ℓ_p -balls: Minimax mean square error. In *2011 IEEE International Symposium on Information
 613 Theory Proceedings*, pp. 129–133. IEEE, 2011.

614 David L Donoho, Arian Maleki, and Andrea Montanari. Message-passing algorithms for com-
 615 pressed sensing. *Proceedings of the National Academy of Sciences*, 106(45):18914–18919, 2009.

616 David L Donoho, Matan Gavish, and Andrea Montanari. The phase transition of matrix recovery
 617 from Gaussian measurements matches the minimax mse of matrix denoising. *Proceedings of the
 618 National Academy of Sciences*, 110(21):8405–8410, 2013.

619 Rishabh Dudeja, Yue M. Lu, and Subhabrata Sen. Universality of approximate message passing
 620 with semirandom matrices. *The Annals of Probability*, 51(5):1616–1683, 2023.

621 Vittorio Erba, Emanuele Troiani, Lenka Zdeborov, and Florent Krzakala. The nuclear route: Sharp
 622 asymptotics of ERM in overparameterized quadratic networks. *NeurIPS 2025*, 2025. arXiv
 623 preprint arXiv:2505.17958.

624 Oliver Y. Feng, Ramji Venkataramanan, Cynthia Rush, and Richard J. Samworth. A unifying tutorial
 625 on approximate message passing. *Foundations and Trends® in Machine Learning*, 15(4):335–
 626 536, 2022. ISSN 1935-8237. doi: 10.1561/2200000092. URL <http://dx.doi.org/10.1561/2200000092>.

627 Cedric Gerbelot and Raphael Berthier. Graph-based approximate message passing iterations. *Infor-
 628 mation and Inference: A Journal of the IMA*, 12(4):2562–2628, 2023.

629 Suriya Gunasekar, Blake E Woodworth, Srinadh Bhojanapalli, Behnam Neyshabur, and Nati Sre-
 630 bro. Implicit regularization in matrix factorization. *Advances in neural information processing
 631 systems*, 30, 2017.

632 Mert Gurbuzbalaban, Umut Simsekli, and Lingjiong Zhu. The heavy-tail phenomenon in sgd. In
 633 *International Conference on Machine Learning*, pp. 3964–3975. PMLR, 2021.

634 Liam Hodgkinson, Umut Simsekli, Rajiv Khanna, and Michael Mahoney. Generalization bounds
 635 using lower tail exponents in stochastic optimizers. In *International Conference on Machine
 636 Learning*, pp. 8774–8795. PMLR, 2022.

637 Liam Hodgkinson, Zhichao Wang, and Michael W Mahoney. Models of heavy-tailed mechanistic
 638 universality. *ICML 2025*, 2025. arXiv preprint arXiv:2506.03470.

648 Jordan Hoffmann, Sébastien Borgeaud, Arthur Mensch, Elena Buchatskaya, Trevor Cai, Eliza
 649 Rutherford, Diego de Las Casas, Lisa Anne Hendricks, Johannes Welbl, Aidan Clark, et al. An
 650 empirical analysis of compute-optimal large language model training. *Advances in neural infor-*
 651 *mation processing systems*, 35:30016–30030, 2022.

652 Jiaoyang Huang. Mesoscopic perturbations of large random matrices. *Random Matrices: Theory*
 653 *and Applications*, 7(02):1850004, 2018.

654 Adel Javanmard and Andrea Montanari. State evolution for general approximate message passing
 655 algorithms, with applications to spatial coupling. *Information and Inference: A Journal of the*
 656 *IMA*, 2(2):115–144, 2013.

657 Jared Kaplan, Sam McCandlish, Tom Henighan, Tom B Brown, Benjamin Chess, Rewon Child,
 658 Scott Gray, Alec Radford, Jeffrey Wu, and Dario Amodei. Scaling laws for neural language
 659 models. *arXiv preprint arXiv:2001.08361*, 2020.

660 Vignesh Kothapalli, Tianyu Pang, Shenyang Deng, Zongmin Liu, and Yaoqing Yang. From spikes
 661 to heavy tails: Unveiling the spectral evolution of neural networks. *Transactions on Machine*
 662 *Learning Research*, 2025.

663 Frederik Kunstner and Francis Bach. Scaling laws for gradient descent and sign descent for linear
 664 bigram models under Zipf’s law. *arXiv preprint arXiv:2505.19227*, 2025.

665 Gen Li and Yuting Wei. A non-asymptotic framework for approximate message passing in spiked
 666 models. *arXiv preprint arXiv:2208.03313*, 2022.

667 Bruno Loureiro, Cédric Gerbelot, Hugo Cui, Sébastien Goldt, Florent Krzakala, Marc Mézard, and
 668 Lenka Zdeborová. Learning curves of generic features maps for realistic datasets with a teacher-
 669 student model. *Advances in Neural Information Processing Systems*, 34:18137–18151, 2021.

670 Michael Mahoney and Charles Martin. Traditional and heavy tailed self regularization in neural
 671 network models. In *International Conference on Machine Learning*, pp. 4284–4293. PMLR,
 672 2019.

673 Antoine Maillard and Dmitriy Kunisky. Fitting an ellipsoid to random points: predictions using the
 674 replica method. *IEEE Transactions on Information Theory*, 70(10):7273–7296, 2024.

675 Antoine Maillard, Florent Krzakala, Marc Mézard, and Lenka Zdeborová. Perturbative construction
 676 of mean-field equations in extensive-rank matrix factorization and denoising. *Journal of Statistical*
 677 *Mechanics: Theory and Experiment*, 2022(8):083301, 2022.

678 Antoine Maillard, Emanuele Troiani, Simon Martin, Florent Krzakala, and Lenka Zdeborová.
 679 Bayes-optimal learning of an extensive-width neural network from quadratically many samples.
 680 *Advances in Neural Information Processing Systems*, 37:82085–82132, 2024.

681 Stéphane Mallat. *A wavelet tour of signal processing*. Elsevier, 1999.

682 Alexander Maloney, Daniel A Roberts, and James Sully. A solvable model of neural scaling laws.
 683 *arXiv preprint arXiv:2210.16859*, 2022.

684 Charles H Martin and Michael W Mahoney. Implicit self-regularization in deep neural networks:
 685 Evidence from random matrix theory and implications for learning. *Journal of Machine Learning*
 686 *Research*, 22(165):1–73, 2021a.

687 Charles H Martin and Michael W Mahoney. Post-mortem on a deep learning contest: a simp-
 688 son’s paradox and the complementary roles of scale metrics versus shape metrics. *arXiv preprint*
 689 *arXiv:2106.00734*, 2021b.

690 Charles H Martin, Tongsu Peng, and Michael W Mahoney. Predicting trends in the quality of state-
 691 of-the-art neural networks without access to training or testing data. *Nature Communications*, 12
 692 (1):4122, 2021.

693 Simon Martin, Francis Bach, and Giulio Biroli. On the impact of overparameterization on the
 694 training of a shallow neural network in high dimensions. In *International Conference on Artificial*
 695 *Intelligence and Statistics*, pp. 3655–3663. PMLR, 2024.

702 Song Mei and Andrea Montanari. The generalization error of random features regression: Precise
 703 asymptotics and the double descent curve. *Communications on Pure and Applied Mathematics*,
 704 75(4):667–766, 2022.

705 Léo Miolane and Andrea Montanari. The distribution of the lasso. *The Annals of Statistics*, 49(4):
 706 2313–2335, 2021.

708 Theodor Misiakiewicz and Basil Saeed. A non-asymptotic theory of kernel ridge regression: deter-
 709 ministic equivalents, test error, and GCV estimator. *arXiv preprint arXiv:2403.08938*, 2024.

710 Behrad Moniri, Donghwan Lee, Hamed Hassani, and Edgar Dobriban. A theory of non-linear
 711 feature learning with one gradient step in two-layer neural networks. *ICML 2024*, 2023. arXiv
 712 preprint arXiv:2310.07891.

713 Sahand Negahban and Martin J. Wainwright. Estimation of (near) low-rank matrices with noise and
 714 high-dimensional scaling. *The Annals of Statistics*, 39(2):1069–1097, 2011. ISSN 00905364,
 715 21688966.

716 Behnam Neyshabur, Ryota Tomioka, and Nathan Srebro. Norm-based capacity control in neural
 717 networks. In *Conference on learning theory*, pp. 1376–1401. PMLR, 2015.

718 Brian Richard Olsen, Sam Fatehmanesh, Frank Xiao, Adarsh Kumarappan, and Anirudh Gajula.
 719 From SGD to spectra: A theory of neural network weight dynamics. *arXiv preprint
 720 arXiv:2507.12709*, 2025.

721 Elliot Paquette, Courtney Paquette, Lechao Xiao, and Jeffrey Pennington. 4+3 phases of compute-
 722 optimal neural scaling laws. *Advances in Neural Information Processing Systems*, 37:16459–
 723 16537, 2024.

724 Scott Pesme and Nicolas Flammarion. Saddle-to-saddle dynamics in diagonal linear networks. *Ad-
 725 vances in Neural Information Processing Systems*, 36:7475–7505, 2023.

726 Sundeep Rangan. Generalized approximate message passing for estimation with random linear
 727 mixing. In *2011 IEEE International Symposium on Information Theory Proceedings*, pp. 2168–
 728 2172, 2011. doi: 10.1109/ISIT.2011.6033942.

729 Garvesh Raskutti, Martin J Wainwright, and Bin Yu. Minimax rates of estimation for high-
 730 dimensional linear regression over ℓ_q -balls. *IEEE transactions on information theory*, 57(10):
 731 6976–6994, 2011.

732 Galen Reeves. Dimension-free bounds for generalized first-order methods via Gaussian coupling.
 733 *arXiv preprint arXiv:2508.10782*, 2025.

734 Yunwei Ren, Eshaan Nichani, Denny Wu, and Jason D Lee. Emergence and scaling laws in SGD
 735 learning of shallow neural networks. *arXiv preprint arXiv:2504.19983*, 2025.

736 Cynthia Rush and Ramji Venkataramanan. Finite sample analysis of approximate message passing
 737 algorithms. *IEEE Transactions on Information Theory*, 64(11):7264–7286, 2018.

738 Stefano Sarao Mannelli, Eric Vanden-Eijnden, and Lenka Zdeborová. Optimization and gener-
 739 alization of shallow neural networks with quadratic activation functions. *Advances in Neural
 740 Information Processing Systems*, 33:13445–13455, 2020.

741 J.W. Silverstein and Z.D. Bai. On the empirical distribution of eigenvalues of a class of large di-
 742 mensional random matrices. *Journal of Multivariate Analysis*, 54(2):175–192, 1995. ISSN 0047-
 743 259X. doi: <https://doi.org/10.1006/jmva.1995.1051>.

744 James B Simon, Madeline Dickens, Dhruva Karkada, and Michael R DeWeese. The eigenlearning
 745 framework: A conservation law perspective on kernel ridge regression and wide neural networks.
 746 *Transactions on Machine Learning Research*, 2023.

747 Umut Simsekli, Ozan Sener, George Deligiannidis, and Murat A Erdogdu. Hausdorff dimension,
 748 heavy tails, and generalization in neural networks. *Advances in Neural Information Processing
 749 Systems*, 33:5138–5151, 2020.

756 Daniel Soudry, Elad Hoffer, Mor Shpigel Nacson, Suriya Gunasekar, and Nathan Srebro. The im-
 757 plicit bias of gradient descent on separable data. *Journal of Machine Learning Research*, 19(70):
 758 1–57, 2018.

759 Stefano Spigler, Mario Geiger, and Matthieu Wyart. Asymptotic learning curves of kernel methods:
 760 empirical data versus teacher–student paradigm. *Journal of Statistical Mechanics: Theory and*
 761 *Experiment*, 2020(12):124001, 2020.

763 Ingo Steinwart, Don R Hush, Clint Scovel, et al. Optimal rates for regularized least squares regres-
 764 sion. In *COLT*, pp. 79–93, 2009.

765 Matthias Thamm, Max Staats, and Bernd Rosenow. Random matrix theory analysis of neural net-
 766 work weight matrices. In *High-dimensional Learning Dynamics 2024: The Emergence of Struc-
 767 ture and Reasoning*, 2024.

769 Yutong Wang, Rishi Sonthalia, and Wei Hu. Near-interpolators: Rapid norm growth and the trade-
 770 off between interpolation and generalization. In *International Conference on Artificial Intelli-
 771 gence and Statistics*, pp. 4483–4491. PMLR, 2024.

772 Zhichao Wang, Andrew Engel, Anand D Sarwate, Ioana Dumitriu, and Tony Chiang. Spectral evo-
 773 lution and invariance in linear-width neural networks. *Advances in neural information processing*
 774 *systems*, 36:20695–20728, 2023.

776 Roman Worschech and Bernd Rosenow. Analyzing neural scaling laws in two-layer networks with
 777 power-law data spectra. *arXiv preprint arXiv:2410.09005*, 2024.

778 Arie Wortsman and Bruno Loureiro. Kernel ridge regression under power-law data: spectrum and
 779 generalization. *arXiv preprint arXiv:2510.04780*, 2025.

781 Yizhou Xu, Antoine Maillard, Lenka Zdeborová, and Florent Krzakala. Fundamental limits of
 782 matrix sensing: Exact asymptotics, universality, and applications. *COLT 2025*, 2025. arXiv
 783 preprint arXiv:2503.14121.

785 Yefan Zhou, Tianyu Pang, Keqin Liu, Michael W Mahoney, Yaoqing Yang, et al. Temperature bal-
 786 ancing, layer-wise weight analysis, and neural network training. *Advances in Neural Information*
 787 *Processing Systems*, 36:63542–63572, 2023.

788 Qiuyun Zou and Hongwen Yang. A concise tutorial on approximate message passing. *arXiv preprint*
 789 *arXiv:2201.07487*, 2022.

791 A THE BRIDGE FROM SPARSE ESTIMATION TO NEURAL NETWORKS

793 A.1 EQUIVALENCE BETWEEN DIAGONAL NETWORKS WITH ℓ_2 WEIGHT DECAY AND LASSO

795 The first equivalence was discussed in a number of papers (Neyshabur et al., 2015; Soudry et al.,
 796 2018; Pesme & Flammarion, 2023). We consider the diagonal two-layer network with parameters
 797 $u, w \in \mathbb{R}^d$ and effective predictor

$$799 \quad \theta = u \odot w, \quad f(x) = \sum_{i=1}^d \theta_i x_i,$$

802 trained with squared loss and ℓ_2 weight decay on both layers:

$$803 \quad \min_{u, w \in \mathbb{R}^d} \frac{1}{2} \|y - X(u \odot w)\|_2^2 + \frac{\lambda}{2} (\|u\|_2^2 + \|w\|_2^2). \quad (21)$$

806 Alternatively, one may also consider a diagonal two-layer ReLU network with two branches per
 807 coordinate:

$$808 \quad f(x) = \sum_{i=1}^d (u_i \sigma(w_i x_i) + u_i \sigma(-w_i x_i)), \quad \sigma(z) = \max\{z, 0\}.$$

810
811 Using $\sigma(z) - \sigma(-z) = z$, each pair of branches along coordinate i induces an effective linear
812 coefficient θ_i such that

$$813 \quad 814 \quad f(x) = \sum_{i=1}^d \theta_i x_i.$$

815 We know show the reduction of this problem to the LASSO one:
816

817 **Step 1. Lower bound via AM–GM.** For each coordinate i we have
818

$$819 \quad u_i^2 + w_i^2 \geq 2|u_i w_i| = 2|\theta_i| \quad (\text{by AM–GM, with } a = u_i^2, b = w_i^2).$$

820 Summing over i gives
821

$$822 \quad \|u\|_2^2 + \|w\|_2^2 \geq 2\|\theta\|_1.$$

823 Therefore, for any factorization with $u \odot w = \theta$,

$$824 \quad 825 \quad \frac{1}{2}\|y - X\theta\|_2^2 + \frac{\lambda}{2}(\|u\|_2^2 + \|w\|_2^2) \geq \frac{1}{2}\|y - X\theta\|_2^2 + \lambda\|\theta\|_1. \quad (22)$$

827 **Step 2. Tightness.** For any θ , choose a factorization
828

$$829 \quad u_i = \text{sign}(\theta_i) |\theta_i|^{1/2}, \quad w_i = |\theta_i|^{1/2}.$$

830 Then $u_i^2 = w_i^2 = |\theta_i|$, so that
831

$$832 \quad u_i^2 + w_i^2 = 2|\theta_i|, \quad u_i w_i = \theta_i.$$

833 Hence equality holds in (22), and the regularizer becomes
834

$$835 \quad \frac{\lambda}{2}(\|u\|_2^2 + \|w\|_2^2) = \lambda\|\theta\|_1.$$

837 Plugging back into (21), we obtain the exact equivalence
838

$$839 \quad \min_{u,w} \frac{1}{2}\|y - X(u \odot w)\|_2^2 + \frac{\lambda}{2}(\|u\|_2^2 + \|w\|_2^2) \equiv \min_{\theta \in \mathbb{R}^d} \frac{1}{2}\|y - X\theta\|_2^2 + \lambda\|\theta\|_1,$$

841 which is precisely the *LASSO* loss.
842

843 A.2 EQUIVALENCE BETWEEN QUADRATIC NETWORKS WITH ℓ_2 WEIGHT DECAY AND 844 MATRIX COMPRESSED SENSING 845

846 Again the equivalence has been discussed in a number of work (Gunasekar et al., 2017; Maillard &
847 Kunisky, 2024; Erba et al., 2025; Bandeira & Maillard, 2025)

848 We consider the two-layer quadratic network with centered activations
849

$$850 \quad 851 \quad f(\mathbf{x}; \mathbf{W}) = \frac{1}{\sqrt{p}} \sum_{j=1}^p \left[(\mathbf{w}_j^\top \mathbf{x})^2 - \mathbb{E}[(\mathbf{w}_j^\top \mathbf{x})^2] \right].$$

853 Centering is equivalent to learning (and absorbing) the constant offset via a bias term, and can also
854 be naturally implemented in practice by batch/layer normalization applied after squaring.
855

856 This network can be written as
857

$$f(\mathbf{x}) = \text{Tr}[\mathbf{S}\mathbf{Z}],$$

858 where $\mathbf{S} := \frac{1}{\sqrt{p}} \mathbf{W} \mathbf{W}^\top \succeq 0$ and $\mathbf{Z} := \mathbf{x} \mathbf{x}^\top - \mathbf{\Sigma}_x$, $\mathbf{\Sigma}_x = \mathbb{E}[\mathbf{x} \mathbf{x}^\top]$. Thus the network corresponds
859 exactly to a PSD matrix sensing model with centered measurements \mathbf{Z} . Centering removes only
860 a constant offset, which in practice would be absorbed by a bias term or handled automatically by
861 batch/layer normalization. Moreover, weight decay on \mathbf{W} induces a trace penalty on \mathbf{S} , since

$$862 \quad \|\mathbf{W}\|_F^2 = \sqrt{p} \text{tr}(\mathbf{S}),$$

863 so that training is equivalent to trace-regularized PSD matrix sensing.

Following the universality results for matrix sensing (see, e.g., [Maillard & Kunisky \(2024\)](#); [Bandeira & Maillard \(2025\)](#); [Maillard et al. \(2024\)](#); [Xu et al. \(2025\)](#); [Erba et al. \(2025\)](#)), the analysis can be simplified by replacing the empirical sensing operators \mathbf{Z} by i.i.d. Gaussian symmetric matrices with matching covariance structure. In particular, for $x_i \sim \mathcal{N}(0, I_d)$, the centered measurements are distributed as rank-one Wishart fluctuations, which are asymptotically equivalent, in the sense of state evolution and AMP analysis, to Gaussian measurements with the same variance. Hence, without loss of generality, we may study the trace-regularized PSD matrix sensing problem with Gaussian measurement operators

$$y_\mu = \text{Tr}[\mathbf{S}\mathbf{G}_\mu] + \xi_\mu, \quad \mathbf{G}_\mu \sim \text{GOE}(d).$$

B DERIVATION DETAILS - DIAGONAL LINEAR NETWORK

Considering the reparametrization defined in Section 1 and detailed in Appendix A, mapping empirical risk minimization with L_2 penalty on a two-layer diagonal linear network to LASSO regression, in this section we study the supervised learning problem

$$\hat{\boldsymbol{\theta}} = \arg \min_{\boldsymbol{\theta} \in \mathbb{R}^d} \left\{ \frac{1}{2} \sum_{\mu=1}^n \left(y_\mu - \frac{\langle \mathbf{x}_\mu, \boldsymbol{\theta} \rangle}{\sqrt{d}} \right)^2 + \lambda \|\boldsymbol{\theta}\|_1 \right\}, \quad (23)$$

with $\mathbf{x}_\mu \sim \mathcal{N}(\mathbf{0}, I_d)$, and

$$y_\mu = \frac{\langle \mathbf{x}_\mu, \boldsymbol{\theta}^* \rangle}{\sqrt{d}} + \sqrt{\Delta} \xi_\mu, \quad \xi_\mu \sim \mathcal{N}(0, 1), \quad \mu = 1, \dots, n \quad (24)$$

$$\boldsymbol{\theta}^* \sim \mathcal{N}(\mathbf{0}, \boldsymbol{\Lambda}), \quad \Lambda_{ij} = \delta_{ij} d i^{-2\gamma} =: \Lambda_i, \quad i = 1, \dots, d \quad (25)$$

We also define the parameter $Q^* = d^{-1} \text{Tr} \boldsymbol{\Lambda} \xrightarrow{d \rightarrow \infty} \zeta(2\gamma)$. The excess risk is defined as

$$R(\hat{\boldsymbol{\theta}}) = \frac{1}{d} \mathbb{E}[(\mathbf{x}^T \hat{\boldsymbol{\theta}} - \mathbf{x}^T \boldsymbol{\theta}^*)^2]. \quad (26)$$

In sections B.1 and B.2 we derive the state evolution equations 45) for the excess risk of the ERM estimator eq. (23) and (57) for the Bayes-optimal estimator in the high-dimensional limit $n, d \rightarrow \infty$ with n/d and λ fixed. Then, in sections B.3 and B.4, assuming the excess risk equations holds for arbitrary scaling between dimensions and regularization, we derive the Results in Section 2.1.

B.1 GENERALIZED APPROXIMATE MESSAGE PASSING AND STATE EVOLUTION

Our theory is built on the analysis of *Generalized Approximate Message Passing* (GAMP) algorithms, tailored for Bayes-optimal estimation and (convex) empirical risk minimization. In this section we provide an overview of the derivation of the expressions for R and the LASSO R in our setting from the GAMP framework.

Consider the matrix $\mathbf{X} \in \mathbb{R}^{n \times d}$, with i.i.d. Gaussian components $X_{ij} \sim \mathcal{N}(0, 1)$, the vectors $\mathbf{b}^t \in \mathbb{R}^d$, $\boldsymbol{\omega}^t \in \mathbb{R}^n$, and the functions (known as *denoisers*) $f_t : \mathbb{R}^d \rightarrow \mathbb{R}^d$ and $g_t : \mathbb{R}^n \rightarrow \mathbb{R}^n$, with $t \geq 1$. The generic form of GAMP ([Donoho et al., 2009](#); [Rangan, 2011](#)) is given by

$$\boldsymbol{\omega}^t = \mathbf{X} f_t(\mathbf{b}^t) - v_t g_{t-1}(\boldsymbol{\omega}^{t-1}), \quad (27)$$

$$\mathbf{b}^{t+1} = \mathbf{X}^T g_t(\boldsymbol{\omega}^t) + a_t f_t(\mathbf{b}^t). \quad (28)$$

The terms a_t and v_t are known in the statistical physics literature as *Onsager terms*, and they are defined as

$$a_t = -\frac{1}{d} \sum_{\mu=1}^n \frac{\partial}{\partial \omega_i} g_t(\boldsymbol{\omega}), \quad v_t = \frac{1}{d} \sum_{i=1}^d \frac{\partial}{\partial b_i} f_t(\mathbf{b}). \quad (29)$$

For separable denoiser functions³, one can track statistics of the iterated vectors \mathbf{b}^t , $\boldsymbol{\omega}^t$, leveraging well-known results from [Bayati & Montanari \(2011\)](#); [Javanmard & Montanari \(2013\)](#), through the so called *state evolution*.

³ $f : \mathbb{R}^d \rightarrow \mathbb{R}^d$ is separable if $\forall i \in \{1, \dots, d\} : [f(\mathbf{b} \in \mathbb{R}^d)]_i = f_i(b_i)$, for some scalar function $f_i : \mathbb{R} \rightarrow \mathbb{R}$

918 B.1.1 GAMP FOR CONVEX OPTIMIZATION
919920 Consider the problem of minimizing the empirical risk with loss $\ell(y, z)$ convex in the second argu-
921 ment and convex penalty $r(\theta)$,

922
$$\arg \min_{\theta \in \mathbb{R}^d} \sum_{\mu=1}^n \ell(y^\mu, \theta^T \mathbf{x}^\mu) + \sum_{i=1}^d r(\theta_i), \quad (30)$$

923
924
925

926 It is possible to design a GAMP algorithm whose fixed points are solutions to the problem defined in
927 (30). A detailed discussion on this approach can be found in [Feng et al. \(2022\)](#). Define the functions
928

929
$$\bar{g}(\omega, y, v) := \text{prox}_{v\ell(y, \cdot)}(\omega), \quad g(\omega, y, v) = \frac{\bar{g}(\omega, y, v) - \omega}{v} \quad (31)$$

930

931
$$f(b, a) := \text{prox}_{\frac{1}{a}r}\left(\frac{b}{a}\right), \quad (32)$$

932

933 where the *proximal operator* of a convex function f is defined as
934

935
$$\text{prox}_f(x) = \arg \min_{z \in \mathbb{R}} \left\{ f(z) + \frac{1}{2}(z - x)^2 \right\}. \quad (33)$$

936
937

938 Then, Proposition 4.4 in [Feng et al. \(2022\)](#), guarantees that, given a fixed point (ω, b) of the GAMP
939 algorithm eq. (27,28) with denoiser functions $g_t(\omega) = g(\omega, y, v_t)$ and $f_t(b) = f(b, a_t)$, the vector
940 $\hat{\theta} := f_t(b)$ is the unique minimizer of (30).941 As mentioned, in the high-dimensional limit $n, d \rightarrow \infty$, with n/d fixed, we can track statistics of
942 the iterated variables through a set of state evolution equations. We stress that the following result
943 hold for the considered linear target function $y = \langle(\theta^*)^T, \mathbf{x}\rangle/\sqrt{d}$.944 **Theorem 1** ([Bayati & Montanari \(2011\)](#); [Javanmard & Montanari \(2013\)](#), informal). *Define*
945

946
$$\begin{cases} \hat{q}^t &= \frac{n}{d} \mathbb{E}_{(z, \omega_t)}[g(\omega_t, z, v_t)^2] \\ \hat{m}^t &= \frac{n}{d} \mathbb{E}_{(z, \omega_t)}[\partial_z g(\omega_t, z, v_t)] \\ \hat{v}^t &= -\frac{n}{d} \mathbb{E}_{(z, \omega_t)}[\partial_\omega g(\omega_t, z, v_t)] \end{cases} \quad \begin{cases} q^{t+1} &= \frac{1}{d} \mathbb{E}_{(\xi, \theta^*)}[\|f(\sqrt{\hat{q}^t} \xi + \hat{m}^t \theta^*, \hat{v}^t)\|^2] \\ m^{t+1} &= \frac{1}{d} \mathbb{E}_{(\xi, \theta^*)}[\langle f(\sqrt{\hat{q}^t} \xi + \hat{m}^t \theta^*, \hat{v}^t), \theta^* \rangle] \\ v^{t+1} &= \frac{1}{d} \mathbb{E}_{(\xi, \theta^*)}[\nabla_b \cdot f(\sqrt{\hat{q}^t} \xi + \hat{m}^t \theta^*, \theta^*, \hat{v}^t)] \end{cases} \quad (34)$$

947
948
949
950

951 where $\xi \sim \mathcal{N}(\mathbf{0}, \mathbf{I}_d)$ and
952

953
$$\begin{pmatrix} z \\ \omega^t \end{pmatrix} \sim \mathcal{N}\left(\begin{pmatrix} 0 \\ 0 \end{pmatrix}, \begin{pmatrix} Q^* & m^t \\ m^t & q^t \end{pmatrix}\right). \quad (35)$$

954
955

956 Then the iterated vectors ω^t and b^t of the GAMP algorithm (27,28), with denoiser functions (31,32),
957 respectively converge weakly to the Gaussian vectors $\Omega^t = \sqrt{q^t - m^t} \mathbf{w} + m^t \mathbf{X} \theta^*$ (with $\mathbf{w} \sim$
958 $\mathcal{N}(\mathbf{0}, \mathbf{I}_n)$) and $\mathbf{B}^t = \hat{m}^t \theta^* + \sqrt{\hat{q}^t} \xi$, in the sense that, for any uniformly pseudo-Lipshitz of order
959 k , deterministic $\phi : (\mathbb{R}^d \times \mathbb{R}^n)^t \times \mathbb{R}^d \rightarrow \mathbb{R}$,

960
$$\phi(\mathbf{b}^0, \omega^0, \mathbf{b}^1, \omega^1, \dots, \omega^{t-1}, \mathbf{b}^t) \xrightarrow{P} \mathbb{E}\phi(\mathbf{B}^0, \Omega^0, \mathbf{B}^1, \Omega^1, \dots, \Omega^{t-1}, \mathbf{B}^t). \quad (36)$$

961
962

963 The previous theorem readily implies that, in the high-dimensional limit, $a_t \simeq \hat{v}^t$, and, given $\hat{\theta}^t \simeq$
964 $f(\mathbf{b}^t, a_t)$,

965
$$\frac{1}{d} \langle \hat{\theta}^t, \theta^* \rangle \simeq m^t, \quad \frac{1}{d} \|\hat{\theta}\|^2 \simeq q^t \quad (37)$$

966
967

968 and the generalization error of the estimator $\hat{y}(\mathbf{x}) = f(\mathbf{x}, \hat{\theta}^t) = \langle \hat{\theta}^t, \mathbf{x} \rangle / \sqrt{d}$ is
969

970
$$R(\hat{\theta}^t) \simeq \mathbb{E}_{\mathbf{x}} \left(\frac{\langle \hat{\theta}^t, \mathbf{x} \rangle}{\sqrt{d}} - \frac{\langle \hat{\theta}^t, \mathbf{x} \rangle}{\sqrt{d}} \right)^2 = Q^* - 2m^t + q^t. \quad (38)$$

971

972 **LASSO regression** In the case of LASSO, with $\ell(y, z) = (y - z)^2/2$ and $r(\theta) = \lambda|\theta|$, we have
 973 that
 974

$$975 \quad g(\omega, y, v) = \frac{y - \omega}{1 + v}, \quad f(b, a) = \frac{1}{a} \text{ST}_\lambda(b), \quad (39)$$

977 where $\text{ST}_\lambda(b) = \max(b - \lambda, 0) - \max(-b - \lambda, 0)$ denotes the soft-thresholding function. The state
 978 evolution equations in this setting read
 979

$$980 \quad \begin{cases} \hat{q}^t &= \frac{n(\Delta + Q^* - 2m^t + q^t)}{d(1+v^t)^2} \\ \hat{m}^t &= \frac{n}{d(1+v^t)} \\ \hat{v}^t &= \frac{n}{d(1+v^t)} \end{cases} \quad \begin{cases} m^{t+1} &= \frac{1}{d} \sum_{i=1}^d \Lambda_i \text{erfc} \left(\frac{\lambda}{\sqrt{2((\hat{m}^t)^2 \Lambda_i + \hat{q}^t)}} \right) \\ v^{t+1} &= \frac{1}{d\hat{m}^t} \sum_{i=1}^d \text{erfc} \left(\frac{\lambda}{\sqrt{2((\hat{m}^t)^2 \Lambda_i + \hat{q}^t)}} \right) \end{cases} \quad (40)$$

984 and
 985

$$986 \quad q^{t+1} = \frac{1}{d(\hat{m}^t)^2} \sum_{i=1}^d \left[((\hat{m}^t)^2 \Lambda_i + \hat{q}^t + \lambda^2) \text{erfc} \left(\frac{\lambda}{\sqrt{2((\hat{m}^t)^2 \Lambda_i + \hat{q}^t)}} \right) \right] \quad (41)$$

$$989 \quad - \frac{1}{d(\hat{m}^t)^2} \sum_{i=1}^d \left[\frac{2\lambda}{\sqrt{2\pi}} \sqrt{(\hat{m}^t)^2 \Lambda_i + \hat{q}^t} e^{-\lambda^2/(2((\hat{m}^t)^2 \Lambda_i + \hat{q}^t))} \right]. \quad (42)$$

992 At convergence, substituting the equation for v into the equation for one for \hat{m} , introducing the parameter
 993 $\nu = \frac{\lambda}{\hat{m}} \sqrt{\frac{n}{2d}}$ and leveraging eq. (38), one obtains that the excess risk for LASSO regression
 994 in this setting is given by

$$995 \quad R(\hat{\theta}) \simeq R_{n,d}(\nu) = \frac{1}{n} \sum_{i=1}^d \left[\frac{n}{d} \Lambda_i \text{erf} \left(\frac{\nu}{\sqrt{\frac{n}{d} \Lambda_i + \hat{\Delta}}} \right) + (\hat{\Delta} + 2\nu^2) \text{erfc} \left(\frac{\nu}{\sqrt{\frac{n}{d} \Lambda_i + \hat{\Delta}}} \right) \right] \\ 996 \quad - \frac{2\nu}{n\sqrt{\pi}} \sum_{i=1}^d \left[\sqrt{\frac{n}{d} \Lambda_i + \hat{\Delta}} e^{-\nu^2/(\frac{n}{d} \Lambda_i + \hat{\Delta})} \right], \quad (43)$$

1002 with $\hat{\Delta} = \Delta + R_{n,d}(\nu)$ and
 1003

$$1004 \quad \frac{\lambda}{\nu} \sqrt{\frac{n}{2d}} + \frac{1}{d} \sum_{i=1}^d \text{erfc} \left(\frac{\nu}{\sqrt{\frac{n}{d} \Lambda_i + \hat{\Delta}}} \right) = \frac{n}{d}. \quad (44)$$

1008 For our specific choice of covariance $\Lambda_i = di^{-2\gamma}$, this becomes
 1009

$$1010 \quad R(\hat{\theta}) \simeq R_{n,d}(\nu) = \frac{1}{n} \sum_{i=1}^d \left[ni^{-2\gamma} \text{erf} \left(\frac{\nu}{\sqrt{ni^{-2\gamma} + \hat{\Delta}}} \right) + (\hat{\Delta} + 2\nu^2) \text{erfc} \left(\frac{\nu}{\sqrt{ni^{-2\gamma} + \hat{\Delta}}} \right) \right] \\ 1011 \quad - \frac{2\nu}{n\sqrt{\pi}} \sum_{i=1}^d \left[\sqrt{ni^{-2\gamma} + \hat{\Delta}} e^{-\nu^2/(ni^{-2\gamma} + \hat{\Delta})} \right], \quad (45)$$

1015 and
 1016

$$1017 \quad \frac{\lambda}{\nu} \sqrt{\frac{n}{2d}} + \frac{1}{d} \sum_{i=1}^d \text{erfc} \left(\frac{\nu}{\sqrt{ni^{-2\gamma} + \hat{\Delta}}} \right) = \frac{n}{d}. \quad (46)$$

1020 **Conjecture 2.** Define $R(\hat{\theta}, \lambda)$ the excess risk eq.(26) of the LASSO estimator $\hat{\theta}$ eq. (23) with
 1021 regularization strength λ . Then, there exists $C > 0$ such that, for any $n, d > C$, with probability
 1022 $1 - o_n(1) - o_d(1)$,
 1023

$$1024 \quad |R(\hat{\theta}, \lambda) - R_{n,d}(\nu(\lambda))| = R_{n,d}(\nu(\lambda)) \cdot o_{n,d}(1), \quad (47)$$

1025 with $R_{n,d}(\nu)$ defined in eq. (45) and $\nu(\lambda)$ solution of eq. (46).

1026

B.1.2 SPECTRAL STRUCTURE OF THE ESTIMATOR

1027

Theorem 1 readily implies Result 2. Given the unique fixed point $(\boldsymbol{\omega}, \mathbf{b})$ of GAMP, the minimizer of eq. (5) is given by $\hat{\boldsymbol{\theta}} = \frac{1}{m} \text{ST}_\lambda(\mathbf{b})$, which satisfies, in distribution

$$\hat{\theta}_i \sim \text{ST}_{\epsilon_d}(\theta_i^* + \delta_d z_i), \quad (48)$$

1031

with $\epsilon_d := \lambda/\hat{m}$, $\delta_d := \sqrt{\hat{q}}/\hat{m}$ and $z_i \sim \mathcal{N}(0, 1)$. Note that $\epsilon_d = \nu\sqrt{d/n}$ and

1032

$$|\hat{\theta}_i| \sim \max \left(\left| \underbrace{\theta_i^* + z_i \sqrt{\hat{\Delta} \frac{d}{n}}}_{=:u_i} \right| - \nu \sqrt{\frac{2d}{n}}, 0 \right). \quad (49)$$

1033

The random variable variable u_i satisfies

1034

$$u_i \sim \mathcal{N} \left(0, d i^{-2\gamma} + \hat{\Delta} \frac{d}{n} \right) \implies u_i \sim \begin{cases} \theta_i^*, & i \ll \min \left(\left(\frac{N}{\hat{\Delta}} \right)^{1/(2\gamma)}, d \right) \\ z_i \sqrt{\hat{\Delta} \frac{d}{n}} & i \gg \left(\frac{N}{\hat{\Delta}} \right)^{1/(2\gamma)}, \text{ if } \left(\frac{N}{\hat{\Delta}} \right)^{1/(2\gamma)} \ll d \end{cases} \quad (50)$$

1041

Therefore, if $\left(\frac{N}{\hat{\Delta}} \right)^{1/(2\gamma)} \ll d$, the ensemble $\{u_i\}_{i \gg (n/\hat{\Delta})^{1/(2\gamma)}}$ constitutes a "bulk" of i.i.d. Gaussian variables, representing the combined effect of label noise and the limited number of samples. In fact, if the sample size is large enough, namely $n \gg d^{2\gamma} \hat{\Delta}$, the effect of the noise becomes undetectable. We refer to the remaining $\{u_i\}_{i \ll (n/\hat{\Delta})^{1/(2\gamma)}}$ as "spikes", representing the components of the true signal $\boldsymbol{\theta}^*$ that we want to learn. Therefore, the scale $i \sim (n/\hat{\Delta})^{1/(2\gamma)}$ represents the number of "learnable" components. The LASSO estimator is then obtained by soft-thresholding the variables u_i , where the parameter ϵ_d represents a cutoff that induces sparsity in the estimator, forcing to zero the smallest components. Note that the cutoff depends on the regularization strength λ only through ν . At this level, we can distinguish the following scenarios: in terms of number of data,

1053

| spikes + bulk | only spikes |
|-----------------------------------|----------------------------------|
| $n \gg d^{2\gamma} \hat{\Delta}$ | $n \gg d^{2\gamma} \hat{\Delta}$ |
| not all components can be learned | all components can be learned |

1054

in terms of thresholding strength,

1055

| weak | strong | extreme |
|--|--|---|
| $\nu^2 \ll \max(nd^{-2\gamma}, \hat{\Delta})$ | $\max(nd^{-2\gamma}, \hat{\Delta}) \ll \nu^2 \ll n$ | $\nu^2 \gg n$ |
| cutoff above all spikes: nothing is learned | cutoff between spikes: signal is partially learned, noise is filtered | cutoff below spikes: all learnable signal is learned |

1056

1057

In Section B.4 we observe that these are the relevant scales for computing the leading order terms of the excess risk and its scaling laws. Moreover, we estimate the values of ν and $\hat{\Delta}$ as functions of n, d, λ . This result can be incorporated to the scenarios we have derived in this section, which will lead us to the identification of the phase diagrams regions in fig. 1 and the phases descriptions in Section 2.2.

1060

B.2 BAYES-OPTIMAL EXCESS RISK

1061

1062

The Bayesian predictor \hat{y}_{BO} is given by the expected value of the target function with respect to the posterior distribution $P(\boldsymbol{\theta}|\mathcal{D})$. Applying Bayes' theorem, the posterior distribution in this setting reads.

1063

1064

1065

$$P(\boldsymbol{\theta}|\mathcal{D}) = \frac{1}{Z(\mathcal{D})} \prod_{i=1}^d \mathcal{N}(\theta_i; 0, \Lambda_i) \prod_{\mu=1}^n \mathcal{N} \left(y_\mu; \frac{1}{\sqrt{d}} \sum_{j=1}^d X_{\mu j} \theta_j, \Delta \right) \quad (51)$$

1066

1067

1068

1069

1070

1071

1072

1073

1074

1075

1076

1077

1078

1079

$$= \mathcal{N}(\boldsymbol{\theta}; \hat{\boldsymbol{\theta}}, \mathbf{V}), \quad (52)$$

1080 where, recalling the notation $\mathbf{X} = (\mathbf{x}_1, \dots, \mathbf{x}_n)^T \in \mathbb{R}^{n \times d}$ for the covariate matrix, $\mathbf{y} =$
 1081 $(y_1, \dots, y_n)^T$ for the label vector and $\mathbf{\Lambda} = \text{diag}(\Lambda_1, \dots, \Lambda_d)$ for the weights' covariance,
 1082

$$1083 \hat{\boldsymbol{\theta}} := \frac{1}{\sqrt{d}\Delta} \mathbf{V} \mathbf{X}^T \mathbf{y}, \quad \mathbf{V} = \left(\mathbf{\Lambda}^{-1} + \frac{1}{d\Delta} \mathbf{X}^T \mathbf{X} \right)^{-1}. \quad (53)$$

1085 Therefore, the Bayesian predictor is $\hat{y}^{\text{BO}}(\mathbf{x}) = \hat{\boldsymbol{\theta}}^T \mathbf{x}$ and its excess risk is given by
 1086

$$1087 R = \mathbb{E}[(\mathbf{x}^T \boldsymbol{\theta}^* - \hat{y}^{\text{BO}}(\mathbf{x}))^2] \quad (54)$$

$$1088 = \mathbb{E}\|\boldsymbol{\theta} - \mathbb{E}_{\boldsymbol{\theta}|\mathcal{D}}[\boldsymbol{\theta}]\|^2 \quad (55)$$

$$1089 = \text{Tr } \mathbf{V}. \quad (56)$$

1090 Leveraging a classical result from random matrix theory [Silverstein & Bai \(1995\)](#), we have that, in
 1091 the high-dimensional limit $n/d \rightarrow \infty$, with fixed ratio n/d ,

$$1093 R = \frac{1}{d} \sum_{i=1}^d \frac{1}{\Lambda_i^{-1} + d^{-1}\hat{q}}, \quad \hat{q} = \frac{n}{\Delta + R} \quad (57)$$

$$1096 = \sum_{i=1}^d \frac{1}{i^{2\gamma} + \hat{q}} \quad (58)$$

1099 The same equations can be derived from the state evolution of Bayes-GAMP, *i.e.* the GAMP algo-
 1100 rithm tailored to compute marginals of the posterior distribution and the Bayes-optimal predictor.
 1101 The interested reader can find a more detailed discussion in Appendix D of [Rangan \(2011\)](#).

1103 B.3 BAYES-OPTIMAL SCALING LAWS

1104 From eq. (57)

$$1106 R = \frac{1}{\hat{q}} \sum_{i=1}^d \frac{1}{1 + (\hat{q}^{-1/(2\gamma)} i)^{2\gamma}}, \quad \hat{q} = \frac{n}{\Delta + R} \quad (59)$$

1109 Our goal is to derive the leading order of R in the asymptotic regime $n, d \gg 1$. The crossover scale
 1110 at which the leading behavior of the sum's argument changes is given by $\hat{q}^{-1/(2\gamma)} i_{\hat{q}} \approx 1 \implies i_{\hat{q}} =$
 1111 $\lfloor \hat{q}^{1/(2\gamma)} \rfloor$. If $i_{\hat{q}} \ll d$, we can split the sum at this relevant scale and retain the leading term for each
 1112 part⁴

$$1114 R = \frac{1}{\hat{q}} \left(\sum_{i=1}^{\lfloor \hat{q}^{1/(2\gamma)} \rfloor} \frac{1}{1 + (\hat{q}^{-1/(2\gamma)} i)^{2\gamma}} + \sum_{\lfloor \hat{q}^{1/(2\gamma)} \rfloor + 1}^d \frac{1}{1 + (\hat{q}^{-1/(2\gamma)} i)^{2\gamma}} \right) \quad (60)$$

$$1117 \approx \frac{1}{\hat{q}} \left(\sum_{i=1}^{\lfloor \hat{q}^{1/(2\gamma)} \rfloor} 1 + \sum_{\lfloor \hat{q}^{1/(2\gamma)} \rfloor + 1}^d \hat{q} i^{-2\gamma} \right) \quad (61)$$

$$1120 \approx \hat{q}^{-1+1/(2\gamma)} + \frac{1}{2\gamma - 1} \hat{q}^{-1+1/(2\gamma)} \quad (62)$$

$$1123 = \frac{2\gamma}{2\gamma - 1} \hat{q}^{-1+1/(2\gamma)}, \quad (63)$$

1125 where we approximate

$$1126 \int_{i_{\hat{q}}+1}^{(d+1)} x^{-2\gamma} dx \leq \sum_{i_{\hat{q}}+1}^d i^{-2\gamma} \leq (i_{\hat{q}} + 1)^{-2\gamma} + \int_{i_{\hat{q}}+1}^{d\hat{q}^{-1/(2\gamma)}} x^{-2\gamma} dx \quad (64)$$

$$1130 \implies \left| \sum_{i_{\hat{q}}+1}^d i^{-2\gamma} - \frac{\hat{q}^{-1+1/(2\gamma)}}{2\gamma - 1} \right| = o_{\hat{q}} \left(\hat{q}^{-1+1/(2\gamma)} \right). \quad (65)$$

1133 ⁴We stress that, throughout the manuscript, the notation \approx denotes equality up to terms that are asymptotically negligible.

1134 If instead $i_{\hat{q}} \gg d$
 1135

1136 $R \approx \frac{1}{\hat{q}} \sum_{i=1}^d 1 = \frac{d}{\hat{q}}$ (66)
 1137
 1138

1139 **Scaling laws** Since $\Delta > 0$, assuming $R = O(1)$, the parameter $\hat{q} \asymp n$ and the Bayes-optimal
 1140 generalization error
 1141

1142 $R = \begin{cases} \Theta(n^{-1/(2\gamma)}), & n \ll d^{2\gamma} \\ \Theta(d/n), & n \gg d^{2\gamma}. \end{cases}$ (67)
 1143
 1144

1145 B.4 LASSO SCALING LAWS
 1146

1147 From eq. (45),
 1148

1149 $R = \frac{1}{n} \sum_{i=1}^d [f_1(x_i) + f_2(x_i) - f_3(x_i)],$ (68)
 1150
 1151

1152 with $x_i := in^{-1/(2\gamma)}$ and
 1153

1154 $f_1(x) = x^{-2\gamma} \operatorname{erf} \left(\frac{\nu}{\sqrt{x^{-2\gamma} + \hat{\Delta}}} \right)$ (69)
 1155
 1156

1157 $f_2(x) = (\hat{\Delta} + 2\nu^2) \operatorname{erfc} \left(\frac{\nu}{\sqrt{x^{-2\gamma} + \hat{\Delta}}} \right)$ (70)
 1158
 1159

1160 $f_3(x) = \frac{2}{\sqrt{\pi}} \nu \sqrt{x^{-2\gamma} + \hat{\Delta}} \exp \left(-\frac{\nu^2}{x^{-2\gamma} + \hat{\Delta}} \right)$ (71)
 1161

1162 We observe that the leading order of the functions changes scale around $x \sim \hat{\Delta}^{-1/(2\gamma)}$.
 1163 For $x^{-2\gamma} \gg \hat{\Delta}$
 1164

1165 $f_1(x) \approx x^{-2\gamma} \operatorname{erf}(\nu x^\gamma)$ (72)

1166 $f_2(x) \approx (\hat{\Delta} + 2\nu^2) \operatorname{erfc}(\nu x^\gamma)$ (73)

1167 $f_3(x) \approx \frac{2}{\sqrt{\pi}} \nu x^{-\gamma} \exp(-\nu^2 x^{2\gamma})$ (74)
 1168
 1169

1170 For $x^{-2\gamma} \ll \hat{\Delta}$
 1171

1172 $f_1(x) \approx x^{-2\gamma} \operatorname{erf}(\nu \hat{\Delta}^{-1/2})$ (75)
 1173
 1174

1175 $f_2(x) \approx (\hat{\Delta} + 2\nu^2) \operatorname{erfc}(\nu \hat{\Delta}^{-1/2})$ (76)
 1176

1177 $f_3(x) \approx \frac{2}{\sqrt{\pi}} \nu \hat{\Delta}^{1/2} \exp(-\nu^2 \hat{\Delta}^{-1}).$ (77)
 1178

1179 Note that the scale $x_i^{-2\gamma} \sim$ corresponds precisely to the detectability threshold of signal components
 1180 observed in Section B.1.2 for the LASSO estimator and in Section B.3 for the Bayes-optimal
 1181 estimator. Following the same procedure of Section B.3, we compute the excess risk R from eq.
 1182 (45) at leading order as a function of the parameter ν , by splitting the sums at the crossover scales.
 1183 Afterwards, solving the self-consistent eq. (46) for ν , we derive the Results in Section 2.1.

1184 The three main regimes are
 1185

1186
$$\begin{cases} \nu \gg x_1^\gamma \implies \nu^2 \gg n, \\ \sqrt{\max(x_d^{-2\gamma}, \hat{\Delta})} \ll \nu \ll x_1^\gamma \implies \max(nd^{-2\gamma}, \hat{\Delta}) \ll \nu^2 \ll n, \\ \nu \ll \sqrt{\max(x_d^{-2\gamma}, \hat{\Delta})} \implies \nu^2 \ll \max(nd^{-2\gamma}, \hat{\Delta}), \end{cases}$$
 (78)
 1187
 1188

which again correspond to the extreme, strong and weak thresholding phases we have identified in Section B.1.2.

In what follows we will often use the expansions

$$\text{erf}(x \ll 1) = \frac{2}{\sqrt{\pi}} x + o(x), \quad (79)$$

$$\text{erfc}(x \gg 1) = \frac{e^{-x^2}}{x\sqrt{\pi}} \left(1 - \frac{1}{2x^2} + \frac{3}{4x^4} + o(x^{-4}) \right). \quad (80)$$

Extreme thresholding For $\nu^2 \gg n$, the dominant term is

$$\frac{1}{n} \sum_{i=1}^d f_1(x_i) \approx \frac{1}{n} \sum_{i=1}^d (x_i)^{-2\gamma} \approx \zeta(2\gamma), \quad (81)$$

while the remaining terms are

$$\frac{1}{n} \sum_{i=1}^d f_2(x_i) - f_3(x_i) \approx \frac{\hat{\Delta}}{\nu\sqrt{n\pi}} \sum_{i=1}^{\min(d, \lfloor (\hat{\Delta}/n)^{-1/(2\gamma)} \rfloor)} i^{-\gamma} e^{-i^2\gamma\nu^2/n} \quad (82)$$

$$\approx \frac{\hat{\Delta}}{\nu\sqrt{n\pi}} \exp(-\nu^2/n), \quad (83)$$

As expected, in this regime the large effective regularization forces the components of the estimator to zero, and $R \approx \zeta(2\gamma)$.

Strong thresholding If instead $\max(nd^{-2\gamma}, \hat{\Delta}) \ll \nu^2 \ll n$, defining $i_\nu := \lfloor (n/\nu^2)^{1/(2\gamma)} \rfloor$ and $i_{\hat{\Delta}} := \lfloor (n/\hat{\Delta})^{1/(2\gamma)} \rfloor$, we split the sums into four terms

$$\begin{aligned} \text{i)} \frac{1}{n} \sum_{i=1}^{i_\nu} f_1(x_i) - f_3(x_i) &\approx \frac{2\nu}{\sqrt{n\pi}} \sum_{i=1}^{i_\nu} (1 - \exp(-i^2\gamma\nu^2/n)) i^{-\gamma} \\ &\approx \frac{2\nu^3}{n\sqrt{n\pi}} \sum_{i=1}^{i_\nu} i^\gamma \\ &\approx \frac{2}{(1+\gamma)\sqrt{\pi}} \left(\frac{n}{\nu^2} \right)^{-1+1/(2\gamma)} \\ \text{ii)} \frac{1}{n} \sum_{i=i_\nu+1}^d f_1(x_i) &\approx \sum_{i=i_\nu+1}^d i^{-2\gamma} \approx \frac{1}{2\gamma-1} \left(\frac{n}{\nu^2} \right)^{-1+1/(2\gamma)} \\ \text{iii)} \frac{1}{n} \sum_{i=1}^{i_\nu} f_2(x_i) &\approx \frac{2\nu^2 + \hat{\Delta}}{n} \sum_{i=1}^{i_\nu} [1 - \text{erf}(i^\gamma\nu/\sqrt{n})] \\ &\approx 2 \left(\frac{n}{\nu^2} \right)^{-1+1/(2\gamma)} + \hat{\Delta} \nu^{-1/\gamma} n^{-1+1/(2\gamma)} + \Theta \left(\left(\frac{n}{\nu^2} \right)^{-1+1/(2\gamma)} \right) \\ \text{iv)} \frac{1}{n} \sum_{i=i_\nu+1}^d f_2(x_i) - f_3(x_i) &\approx \frac{\hat{\Delta}}{\nu\sqrt{n\pi}} \sum_{i=i_\nu+1}^{\min(d, i_{\hat{\Delta}})} i^{-\gamma} e^{-i^2\gamma\nu^2/n} + \mathbf{1}_{[\hat{\Delta} > nd^{-2\gamma}]} \frac{d\hat{\Delta}^{5/2}}{n\nu^3} e^{-\nu^2/\hat{\Delta}} \\ &\stackrel{\text{Laplace}}{\approx} \frac{\hat{\Delta}}{e\sqrt{\gamma(2\gamma-1)}} n^{-1+1/(2\gamma)} \nu^{-1/\gamma} + \mathbf{1}_{[\hat{\Delta} > nd^{-2\gamma}]} \frac{d\hat{\Delta}^{5/2}}{n\nu^3} \exp \left(-\frac{\nu^2}{\hat{\Delta}} \right) \end{aligned}$$

where in the last step we have approximated the (Riemann) sum by an integral which we solved using the Laplace's method, that is (informally)

$$\int_a^b h(x) e^{Mg(x)} dx \stackrel{M \gg 1}{\approx} \sqrt{\frac{2\pi}{M|g''(x_0)|}} h(x_0) e^{Mg(x_0)}, \quad x_0 = \arg \max_{x \in [a, b]} g(x), \quad g''(x) \leq 0 \forall x \in [a, b]. \quad (84)$$

For $\nu^2/\hat{\Delta}$ larger than any polylogarithmic function of n, d , the dominant term is $R \asymp (n/\nu^2)^{-1+1/(2\gamma)}$; if instead $\nu^2/\hat{\Delta}$ is polylogarithmic in n, d , one should also take into account

1242 the term $\frac{d\hat{\Delta}^{5/2}}{n\nu^3} \exp\left(-\frac{\nu^2}{\hat{\Delta}}\right)$. Note that this last contribution comes from the summation over the
 1243 "bulk components" $i > i_{\hat{\Delta}}$, therefore it represent the noise-fitting contribution to the excess risk,
 1244 when the thresholding parameter $\epsilon_d = \nu\sqrt{d/n}$ is comparable the square root of the bulk variance
 1245 $\delta_d = \sqrt{\hat{\Delta}d/n}$ and a non negligible amount of bulk components does not get filtered.
 1246

1247
 1248 **Weak thresholding** Finally, if $\nu^2 \ll \max(nd^{-2\gamma}, \hat{\Delta})$, we split the sums into the following four
 1249 terms
 1250

$$\begin{aligned}
 \text{i) } & \frac{1}{n} \sum_{i=1}^{\min(i_{\hat{\Delta}}, d)} f_1(x_i) - f_3(x_i) \approx \frac{2\nu^3}{(1+\gamma)\sqrt{n\pi}} \left(\mathbf{1}_{[\hat{\Delta} > nd^{-2\gamma}]} \left(\frac{n}{\hat{\Delta}} \right)^{(1+\gamma)/(2\gamma)} + \mathbf{1}_{[\hat{\Delta} < nd^{-2\gamma}]} d^{1+\gamma} \right) \\
 \text{ii) } & \frac{1}{n} \sum_{i=\min(d, i_{\hat{\Delta}}+1)}^d f_1(x_i) \approx \mathbf{1}_{[\hat{\Delta} > nd^{-2\gamma}]} \frac{2\nu}{\sqrt{\hat{\Delta}\pi}} \sum_{i=i_{\hat{\Delta}}+1}^d i^{-2\gamma} \\
 & \approx \mathbf{1}_{[\hat{\Delta} > nd^{-2\gamma}]} \frac{2\nu}{\sqrt{\hat{\Delta}\pi}} \left(\frac{n}{\hat{\Delta}} \right)^{-1+1/(2\gamma)} \\
 \text{iii) } & \frac{1}{n} \sum_{i=1}^d f_2(x_i) \approx (2\nu^2 + \hat{\Delta}) \min \left(n^{-1+1/(2\gamma)} \hat{\Delta}^{-1/(2\gamma)}, \frac{d}{n} \right) + \mathbf{1}_{[\hat{\Delta} > nd^{-2\gamma}]} \left(\frac{d}{n} - n^{-1+1/(2\gamma)} \hat{\Delta}^{-1/(2\gamma)} \right) \\
 & = (2\nu^2 + \hat{\Delta}) \frac{d}{n} \\
 \text{iv) } & \frac{1}{n} \sum_{i=\min(d, i_{\hat{\Delta}}+1)}^d -f_3(x_i) \approx -\mathbf{1}_{[\hat{\Delta} > nd^{-2\gamma}]} \frac{2}{\sqrt{\pi}} \nu \sqrt{\hat{\Delta}} \exp(-\nu^2/\hat{\Delta}) \frac{d}{n}
 \end{aligned} \tag{85}$$

1268 The dominant term is therefore $R \asymp (2\nu^2 + \hat{\Delta})d/n$.
 1269 We can now proceed with the solution of the self-consistent equation (46), in order to derive the
 1270 closed-form expressions for the excess risk scaling laws.

1271
 1272 **Scaling Laws** Since $\Delta > 0$, then, provided $R = O(1)$, $\hat{\Delta} = \Theta(1)$. Let $n \gg d$. Eq. (46) readily
 1273 implies that $\nu \asymp \lambda\sqrt{d/n}$, as the second term on the left-hand side is bounded by 1. Therefore, for
 1274 $n \gg d$,

$$R = \begin{cases} \Theta(1), & \lambda \gg n/\sqrt{d}, \\ \Theta\left(\frac{n^2}{\lambda^2 d}\right)^{-1+1/(2\gamma)}, & \max(nd^{-\gamma-1/2}, \sqrt{n/d}) \ll \lambda \ll n/\sqrt{d} \\ \Theta\left(\frac{d}{n} \max\left(1, \frac{\lambda^2 d}{n}\right)\right), & \lambda \ll \max(nd^{-\gamma-1/2}, \sqrt{n/d}) \end{cases} \tag{86}$$

1280 Let instead $n \ll d$. The second term on the left-hand side of eq. (46) is
 1281

$$\frac{1}{d} \sum_{i=1}^d \operatorname{erfc}\left(\frac{\nu}{\sqrt{x^{-2\gamma} + \hat{\Delta}}}\right) \approx \begin{cases} \sqrt{\frac{n}{\pi}} \nu^{-1} \exp(-\nu^2/n), & \nu^2 \gg n, \\ 2 \frac{n^{1/(2\gamma)}}{d} (\nu^{2-1/\gamma}) (1 + O(1)) + \operatorname{erfc}\left(\frac{\nu}{\hat{\Delta}}\right), & 1 \ll \nu^2 \ll n, \\ 1, & \nu \ll 1. \end{cases} \tag{87}$$

1288 For $\lambda \gg \sqrt{n/d}$, this term is subleading and $\nu \asymp \lambda\sqrt{d/n}$. One can observe that eq. (46) does
 1289 not have a positive solution in this regime if $\nu \ll 1$, therefore we exclude this case. Hence, if
 1290 $\lambda \ll \sqrt{n/d}$,

$$\operatorname{erfc}\left(\frac{\nu}{\hat{\Delta}}\right) \approx \frac{n}{d} \implies \sqrt{\frac{\hat{\Delta}}{\pi}} \nu^{-1} e^{-\nu^2/\hat{\Delta}} \approx n/d \tag{88}$$

$$\implies \frac{\nu^2}{\hat{\Delta}} \approx \log \frac{d}{n}, \tag{89}$$

1296 where we used
 1297

1298
 1299 $xe^{x^2} = a \implies 2x^2 e^{2x^2} = 2a^2 \implies x^2 = \frac{1}{2} W_0(2a^2) \stackrel{a \gg 1}{\approx} \frac{1}{2} \log(2a^2) \approx \log a,$ (90)
 1300

1301
 1302 with W_0 denoting the principal branch of the Lambert W function. Note that, in the under-
 1303 parametrized regime $n \ll d$, even a small regularization strength λ leads to large effective
 1304 regularization ν of order $\sqrt{\log d}$.

1305
 1306 We can conclude that, for $n \ll d$
 1307

1308
 1309 $R = \begin{cases} \Theta(1), & \lambda \gg n/\sqrt{d}, \\ \Theta\left(\frac{n^2}{\lambda^2 d}\right)^{-1+1/(2\gamma)}, & \max(nd^{-\gamma-1/2}, \sqrt{n/d}) \ll \lambda \ll n/\sqrt{d} \\ \Theta\left(\left(\frac{n}{\log(d/n)}\right)^{-1+1/(2\gamma)} + \frac{\Delta}{\log(d/n)}\right), & \lambda \ll \sqrt{n/d} \end{cases}$ (91)
 1310
 1311
 1312
 1313

1314
 1315 **Interpolation peak** Around $n \sim d$ the excess risk exhibits an interpolation peak that diverges as
 1316 $\lambda \rightarrow 0^+$. In this section we show that in this regime $R \asymp \lambda^{-2/3}$.
 1317 The self-consistent equation (46) becomes

1318
 1319
 1320 $\frac{\lambda}{\nu} \approx \frac{\sqrt{2}}{d} \sum_{i=1}^d \operatorname{erf}\left(\frac{\nu}{\sqrt{ni^{-2\gamma} + \hat{\Delta}}}\right).$ (92)
 1321
 1322

1323
 1324 As we have done in the previous paragraph, it is easy to verify that a strong effective regularization
 1325 $\nu^2 \gg \hat{\Delta}$ results in the right-hand side being $\Theta(1)$, and to the inconsistent solution $\nu \sim \lambda$. Hence,
 1326 taking $\nu^2 \ll \hat{\Delta}$ (weak thresholding regime),
 1327

1328
 1329 $\frac{\lambda}{\nu} \approx \frac{2\sqrt{2}\nu}{\sqrt{\pi}\hat{\Delta}} \implies \nu^2 \approx \frac{\sqrt{\pi}}{2\sqrt{2}} \frac{\lambda}{\hat{\Delta}}$ (93)
 1330
 1331

1332 $\nu^2 \asymp \lambda\sqrt{\hat{\Delta}}$ and the excess risk becomes, asymptotically,

1333
 1334
 1335 $R \approx 2\nu^2 + R + \Delta - \frac{4}{\sqrt{\pi}}\nu\sqrt{R + \Delta}$ (94)
 1336
 1337

1338 $\implies \nu\sqrt{R + \Delta} \approx \frac{\sqrt{\pi}}{4}\Delta$ (95)
 1339

1340 $\implies \lambda^2(R + \Delta)^3 \approx \frac{\pi^2}{256}\Delta^4$ (96)
 1341

1342 $\implies R \sim \frac{\Delta^{4/3}}{\lambda^{2/3}}.$ (97)
 1343

1344
 1345 B.4.1 ADDITIONAL NUMERICAL SIMULATIONS
 1346

1347
 1348 In this section, we include additional numerical experiments, visualizing the Results in Sections 2.1
 1349 (Fig. 6) and 2.2 (Figs. 4,5). The remarkable correspondence between simulations and all results
 derived from state evolution equations further supports our Conjecture 2.

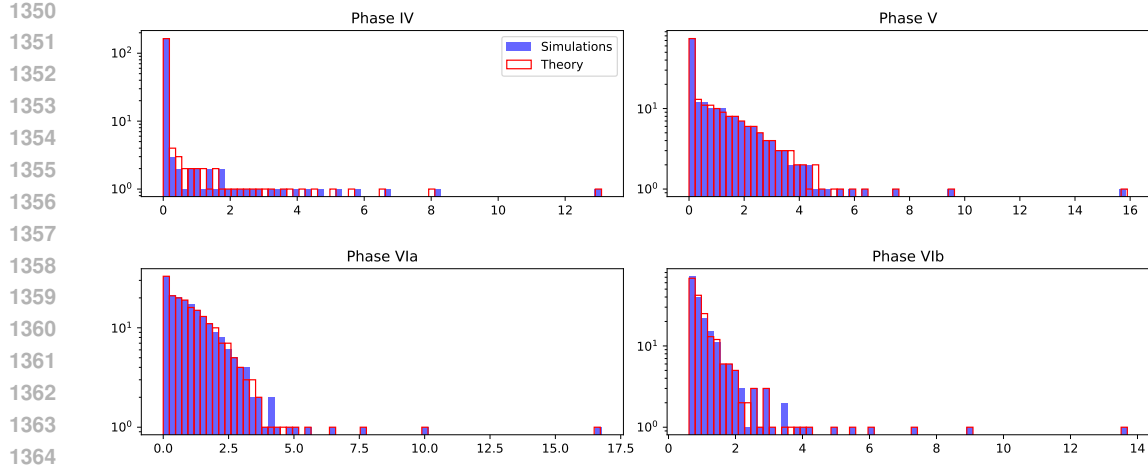


Figure 4: Comparison between spectra from simulations and theory across different training phases. Blue: LASSO estimator’s components (in absolute value) histograms after training. Red: theoretical prediction eq. (48). All panels use $d = 200$ and $\lambda = d^{-1/2}$. The sample size is $n = 35$ for Phase IV, $n = 150$ for Phase V, $n = 300$ for Phase VIa and $n = 3000$ for Phase Ib. We discuss the phenomenology in Section 2.3.

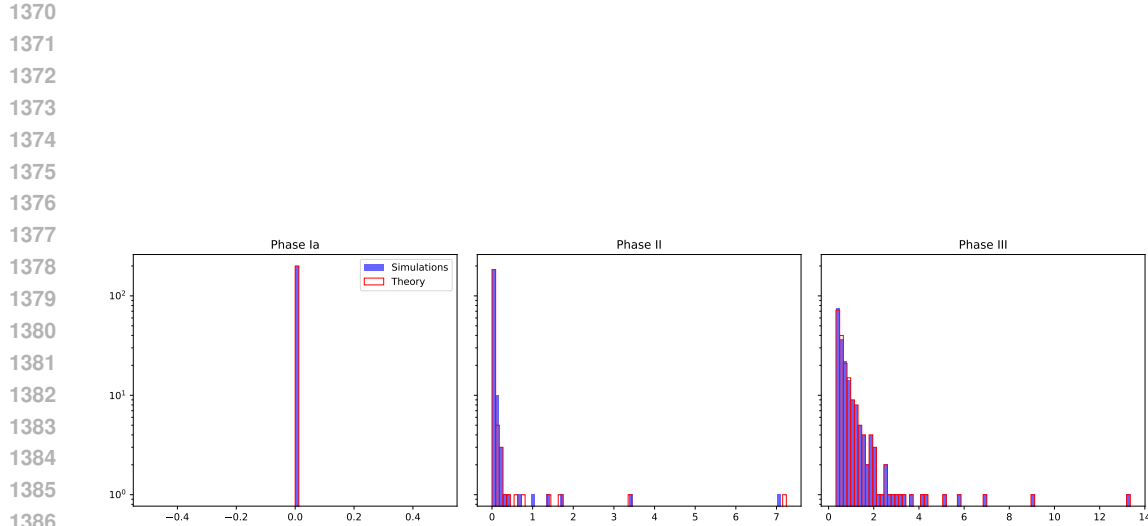


Figure 5: Comparison between spectra from simulations and theory across different training phases. Blue: LASSO estimator’s components (in absolute value) histograms after training. Red: theoretical prediction eq. (48). All panels use $d = 200$ and $n = 100$, $\lambda = 35$ for Phase Ib, $n = 100$, $\lambda = 5.5$ for Phase II, $n = 3000$, $\lambda = 7$ for Phase III. We discuss the phenomenology in Section 2.3.

Figure 6 (left) shows the transitions between phases along the vertical lines of Fig. 1. For example, for $n = 35$ the excess risk moves from Phase IV, which is independent of regularization, into Phase II and soon ($\lambda \approx 35/\sqrt{200}$) enters the plateau region of Phase Ib. For $n = 300$ and $n = 500$, the excess risk starts in the fast-decay region IVa, reaches its minimum at $\lambda \approx \sqrt{n/d}$ (when the soft-thresholding cutoff reaches the edge of the noise bulk, see Section 2.2), then crosses Phase II and enters the plateau Phase Ib. Finally, for $n = 3000$, the excess risk begins in Phase IVb, the fastest decay regime, since the noise bulk is negligible for $n \gg d^{2\gamma}$, then grows as it crosses Phase III and Phase II before reaching the plateau in Phase Ib. Notably, for $n = d = 200$, we observe the interpolation phenomenon when $\lambda < \sqrt{n/d} = 1$, with a peak that grows as the predicted $\lambda^{-2/3}$ in the limit $\lambda \rightarrow 0^+$.

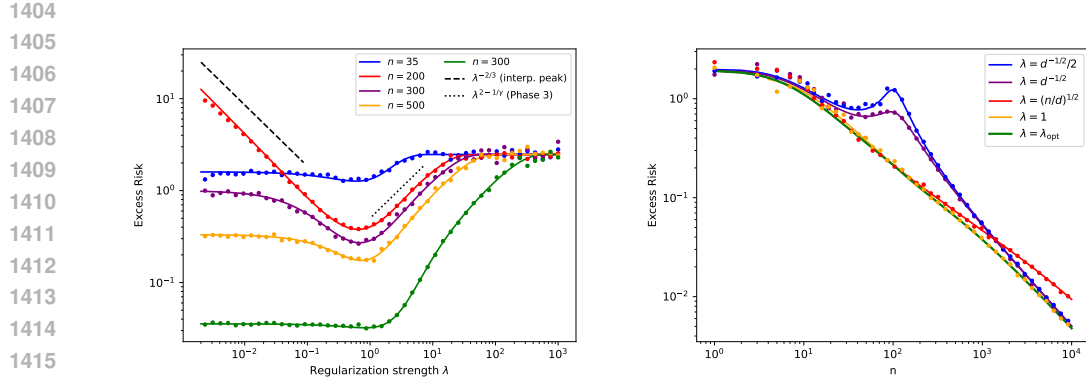


Figure 6: **(Left)** Excess risk of the LASSO estimator, as a function of the regularization strength λ , with $d = 200$, $\Delta = 0.5$, $\gamma = 0.75$. Dots represent numerical experiments, while lines the solution $R_{n,d}$ of state evolution equations 45. The curves correspond to the crossovers between rates observed in Fig. 1. **(Right)** Excess risk of the LASSO estimator, as a function of the sample size n , with $d = 100$, $\Delta = 0.5$, $\gamma = 1$. The regularization λ_{opt} has been chosen as the minimizer of the theoretical excess risk $R_{n,d}$ and its value is in accordance with to Corollary 1. Dots represent numerical experiments, while lines the solution of state evolution equations 45.

C DERIVATION DETAILS - QUADRATIC NEURAL NETWORKS

C.1 BBP SIMPLIFICATION

To derive our results, we make the following assumption, which for the moment we do not control rigorously. We assume that for the sake of simplifying the equations that S^* has sub-extensive rank, i.e. it has eigenvalues $\{\sqrt{d}i^{-\gamma}\}_{i=1}^{cd}$ for $c \ll 1$, and zero otherwise. This technical assumption allows for a great simplification of the density μ_δ (the spectrum of $S^* + \delta Z$, where $Z \sim \text{GOE}(d)$), which can be computed with BBP-like techniques as (Huang, 2018)

$$\mu_\delta(x) = \left(1 - \frac{K}{d}\right)(\mu_{\text{sc}} + o(1))(x/\delta)/\delta + \frac{1}{d} \sum_{i=1}^K \delta(x - f_\delta(\sqrt{d}i^{-\gamma})), \quad (98)$$

We then send $c \rightarrow 1$ *a posteriori*, after finding that the error does not depend explicitly on c . For the rest of the section, let us define $\tilde{\alpha} := n/d^2$.

C.2 BAYESIAN ESTIMATOR

In this section we solve eq. (19) for $\Delta > 0$.

Phase I: Large-samples Phase I is $n \gg d^{2\gamma+1}$. The first equation of eq. (19) gives $\hat{q} = \Theta(n/d^2)$, and thus $d^{\frac{1}{2}-\gamma} \gg \frac{1}{\sqrt{\hat{q}}}$, so all the spikes are outside the bulk. We then have

$$\frac{4\pi^2}{3\hat{q}} \int \mu_{1/\sqrt{\hat{q}}}(x)^3 dx \approx \left(1 - \frac{cd}{d}\right) \frac{4\pi^2}{3} \int \mu_{\text{sc}}(x)^3 dx = 1 - c \quad (99)$$

by eq. (98), and thus eq. (19) gives

$$2\tilde{\alpha}\Delta = \frac{2\tilde{\alpha}\Delta}{\Delta + 2(Q^* - q)}, \quad (100)$$

which gives $R^{\text{BO}} := Q^* - q = \frac{\Delta cd^2}{4n} = \Theta(d^2/n)$.

Phase II: Under-sampling Phase II is $d \ll n \ll d^{2\gamma+1}$. We rewrite the integral in eq. (19) as

$$\frac{4\pi^2}{3\hat{q}} \int \mu_{1/\sqrt{\hat{q}}}(x)^3 dx = \frac{4\pi^2}{3} \int \nu(x)^3 dx = 4\pi^2 \int dx \nu(x)(H[\nu](x))^2, \quad (101)$$

1458 where ν denotes the spectrum density of $Z + \sqrt{q}\Theta^*$. The first equality is by change of variables and
 1459 the second quality is from (Maillard et al., 2022, Lemma C.1). $H[\nu]$ denotes the Hilbert transform
 1460 of ν .

1461 We further denote $\delta := \sqrt{\hat{q}d}$. The first equation of eq. (19) suggests that $\hat{q} = \Theta(n/d^2)$, and thus
 1462 $\delta = \Theta(\sqrt{n/d})$. For $d \ll n \ll d^{2\gamma+1}$ we have $d^{-\gamma+\frac{1}{2}} \ll \delta \ll \sqrt{d}$, so according to eq. (98) ν
 1463 is composed of a semicircle part (denoted as $\nu_0 := (1 - K/d)(\mu_{\text{sc}} + \tilde{\nu})$, where $\tilde{\nu}$ is calculated in
 1464 Appendix C.5) and a discrete part ($\{x_i := f_1(\delta i^{-\gamma})\}_{i=1}^K$, where $K := \delta^{1/\gamma}$). Thus we have
 1465

$$\begin{aligned} 1466 \int dx \nu(x) (H[\nu](x))^2 &= \int dx \nu_0(x) H[\nu_0](x)^2 + \frac{2}{d} \sum_{i=1}^K \int dx \nu_0(x) H[\nu_0](x) \frac{1}{\pi(x - x_i)} \\ 1467 &+ \frac{1}{d^2} \sum_{i,j=1}^K \int dx \nu_0(x) \frac{1}{\pi^2(x - x_i)(x - x_j)} + \sum_{j=1}^K \frac{1}{d} \left(H[\nu_0](x_j) + \sum_{\substack{i=1 \\ i \neq j}}^K \frac{1}{\pi d(x_j - x_i)} \right)^2. \\ 1468 \end{aligned} \quad (102)$$

1474 Denote the right side as $I_1 - I_4$. For the first term we have
 1475

$$I_1 \approx \frac{1}{3} \int dx \mu_{\text{sc}}^3(x) \left(1 - \Theta \left(\frac{1}{d} \sum_{i=K}^{cd} \delta^2 i^{-2\gamma} \right) \right) (1 - 3K/d) \approx \frac{1}{4\pi^2} \left(1 - \Theta(\delta^{1/\gamma} d^{-1}) \right), \quad (103)$$

1479 where we use eq. (171). Then we can estimate the leading orders of the other three terms. For the
 1480 second term, we have

$$I_2 \approx -\frac{2}{d} \int dx \mu_{\text{sc}}(x) \frac{x}{2\pi} \sum_{i=1}^K \frac{1}{x_i} = o \left(d^{-1} \sum_{i=1}^K \frac{1}{x_i} \right) = o(\delta^{1/\gamma} d^{-1}), \quad (104)$$

1484 where we use $H[\mu_{\text{sc}}] = \frac{x}{2\pi}$ for $x \in [-2, 2]$ and the fact that $x\mu_{\text{sc}}$ is an odd function. For the third
 1485 term we have

$$I_3 = \Theta \left(d^{-2} \sum_{i,j=1}^K \frac{1}{x_i x_j} \right) = \Theta \left(\left(d^{-1} \sum_{i=1}^K \frac{1}{x_i} \right)^2 \right) = \Theta(\delta^{2/\gamma} d^{-2}). \quad (105)$$

1489 I_4 is composed of three terms. The first term is
 1490

$$\frac{1}{d} \sum_{j=1}^K (H[\nu_0](x_j))^2 \approx \frac{1}{d} \sum_{j=1}^K x_j^{-2} \approx \frac{1}{\delta^2 d} K^{2\gamma+1} \int_0^1 \frac{x^{2\gamma}}{(1+x^{2\gamma})^2} dx = \Theta(\delta^{1/\gamma} d^{-1}), \quad (106)$$

1494 where we use the fact that $H[\mu_{\text{sc}}](x) \approx \frac{1}{x}$ for $x \gg 1$. The second term of I_4 is
 1495

$$\begin{aligned} 1496 \sum_{\substack{i,j=1 \\ i \neq j}}^K \frac{2}{d^2} H[\nu_0](x_j) \frac{1}{\pi(x_j - x_i)} &\approx \sum_{\substack{i,j=1 \\ i \neq j}}^K \frac{2}{\pi d^2} \frac{1}{x_j(x_j - x_i)} \\ 1497 &= \sum_{\substack{i,j=1 \\ i \neq j}}^K \frac{1}{\pi d^2} \left(\frac{1}{x_j(x_j - x_i)} + \frac{1}{x_i(x_i - x_j)} \right) \\ 1498 &= \sum_{\substack{i,j=1 \\ i \neq j}}^K \frac{1}{\pi d^2 x_i x_j} = \frac{1}{\pi d^2} \left(\sum_{i=1}^K \frac{1}{x_i} \right)^2 = \Theta(\delta^{2/\gamma} d^{-2}). \\ 1499 \end{aligned} \quad (107)$$

1506 The last term of I_4 can be written as
 1507

$$\frac{1}{d^3} \sum_{\substack{i,j,k=1 \\ i \neq j, k}}^K \frac{1}{(x_j - x_i)(x_k - x_i)} \approx \frac{1}{\delta^2 d^3} \sum_{\substack{i,j,k=1 \\ i \neq j, k}}^K \frac{1}{(j^{-\gamma} - i^{-\gamma})(k^{-\gamma} - i^{-\gamma})} \approx \frac{1}{\delta^2 d^3} \sum_{i=1}^K \sum_{m,n} \frac{i^{2\gamma+2}}{m n \gamma^2} \quad (108)$$

1512 where we assuming $m, n \ll i$ to obtain the leading term. For a fixed i , we sum over $m, n =$
 1513 $-(i-1), \dots, -1, 1, \dots, K-i$, which gives
 1514

$$1515 \sum_{i=1}^K \sum_{p,q} \frac{i^{2\gamma+2}}{pq} = \sum_{i=1}^K i^{2\gamma+2} (H_{K-i} - H_{i-1}^2) \approx K^{2\gamma+3} \int_0^1 x^{2\gamma} \left(\log \frac{1-x}{x} \right)^2 dx, \quad (109)$$

1518 where we denote $H_i = \sum_{p=1}^i \frac{1}{p} = \log i + \Theta(1)$. Thus we have
 1519

$$1520 \frac{1}{d^3} \sum_{\substack{i,j,k=1 \\ i \neq j, k}}^K \frac{1}{(x_j - x_i)(x_k - x_i)} = \Theta(\delta^{-2} d^{-3} K^{2\gamma+3}) = \Theta(\delta^{3/\gamma} d^{-3}). \quad (110)$$

1524 For $d \ll n \ll d^{2\gamma+1}$ and $\gamma > \frac{1}{2}$ we have $\delta^{1/\gamma} d^{-1} \ll 1$, and thus
 1525

$$1526 \frac{4\pi^2}{3} \int \nu(y)^3 dy = 1 + \Theta(d^{-1} \delta^{1/\gamma}). \quad (111)$$

1528 Taking it back to (19), we have
 1529

$$1530 \frac{2\tilde{\alpha}\Delta}{\Delta + 2(Q^* - q)} - 2\tilde{\alpha} = \Theta \left(d^{-1} \left(\frac{4n}{d\Delta} \right)^{\frac{1}{2\gamma}} \right), \quad (112)$$

1533 which gives

$$1534 \mathsf{R}^{\text{BO}} := Q^* - q = \Theta \left(\left(\frac{d\Delta}{4n} \right)^{1-\frac{1}{2\gamma}} \right). \quad (113)$$

1538 **Phase III: Not enough data** Phase III is $n \ll d$, and thus $\delta \ll 1$. By eq. (98) and Appendix C.5,
 1539 there are no outliers and the first-order correction reads

$$1540 \frac{4\pi^2}{3} \int \nu(x)^3 dx = 1 - \frac{1}{d} \sum_{i=1}^{cd} (\delta i^{-\gamma})^2 = 1 - \zeta(2\gamma) \hat{q}. \quad (114)$$

1543 Taking it back to eq. (19), we have
 1544

$$1545 \frac{2\tilde{\alpha}\Delta}{\Delta + 2(Q^* - q)} - 2\tilde{\alpha} = -\frac{4\tilde{\alpha}Q^*}{\Delta + 2(Q^* - q)}, \quad (115)$$

1547 and thus $\mathsf{R}^{\text{BO}} := Q^* - q = Q^*$, where we use $Q^* \approx \zeta(2\gamma)$.
 1548

1549 C.3 ERM

1551 In this section we solve eq. (20) for $\Delta > 0$.
 1552

1553 **Phase I: Trivial phase** The first case of phase I is $\delta > \sqrt{d}$ and $0 < 2 - \frac{\lambda\epsilon}{\delta} \ll 1$. In this case the
 1554 spikes are covered by the bulk and the cutoff is close to the boundary of the bulk. Thus we have
 1555

$$1556 J(\delta, \lambda\epsilon) \approx \int_{\lambda\epsilon}^{\delta} \mu_{\text{sc}}(x/\delta)/\delta (x - \lambda\epsilon)^2 dx \approx \delta^2 \frac{16t^{7/2}}{105\pi}, \quad (116)$$

1558 where $t := 2 - \frac{\lambda\epsilon}{\delta}$. Then eq. (20) reduces to
 1559

$$1560 \begin{cases} 4\alpha\delta - \frac{\delta}{\epsilon} = \delta^2 \frac{16t^{5/2}}{15\pi} \\ Q^* + \frac{\Delta}{2} + 2\alpha\delta^2 - \frac{\delta^2}{\epsilon} = \delta^2 \frac{16t^{5/2}}{15\pi}, \end{cases} \quad (117)$$

1563 where we use $t \ll 1$ and keep only the leading term. Thus we have
 1564

$$1565 \mathsf{R} := 2\tilde{\alpha}\delta^2 - \frac{\Delta}{2} = Q^* \quad (118)$$

1566 and $\lambda\epsilon \approx 2\delta = \sqrt{\frac{1}{2\alpha}(Q^* + \Delta/2)}$. Then the condition $\delta > \sqrt{d}$ gives
 1567

$$1568 \quad n < \frac{1}{16}(2Q^* + \Delta)d. \quad (119)$$

1570 The condition $0 < t \ll 1$ gives $\frac{\lambda}{2} \approx \frac{\delta}{\epsilon} < 4\tilde{\alpha}\delta$, and thus
 1571

$$1572 \quad \lambda < 8\sqrt{\frac{2Q^* + \Delta}{4}}\sqrt{\frac{n}{d^2}}. \quad (120)$$

1575 The second case of phase I is $\lambda\epsilon > 2 \max(\delta, \sqrt{d})$. In this case both the spikes and the bulk are
 1576 below the cutoff, and thus $J(\delta, \lambda\epsilon) = 0$. Then eq. (20) reduces to
 1577

$$1578 \quad \begin{cases} 4\alpha\delta - \frac{\delta}{\epsilon} = 0 \\ Q^* + \frac{\Delta}{2} + 2\alpha\delta^2 - \frac{\delta^2}{\epsilon} = 0 \end{cases} \quad (121)$$

1580 which gives
 1581

$$1582 \quad R := 2\tilde{\alpha}\delta^2 - \frac{\Delta}{2} = Q^* \quad (122)$$

1584 and $\epsilon = \frac{1}{4\tilde{\alpha}}$. The condition $\lambda\epsilon > 2 \max(\delta, \sqrt{d})$ reduces to
 1585

$$1586 \quad \lambda > \max\left(8\sqrt{\frac{2Q^* + \Delta}{4}}\sqrt{\frac{n}{d^2}}, \frac{4n}{d^{3/2}}\right). \quad (123)$$

1588 To conclude, Phase I is
 1589

$$1590 \quad R = Q^*, \quad \text{if } n < \frac{1}{16}(2Q^* + \Delta)d \quad \text{or} \quad \lambda > \frac{4n}{d^{3/2}}. \quad (124)$$

1593 **Phase II: Over-regularization phase** The second phase is $\max(\delta, d^{-\gamma+1/2}) \ll \lambda\epsilon \ll \sqrt{d}$. In
 1594 this case we only need to consider the spikes outside the cutoff, so we have
 1595

$$1596 \quad J(\delta, \lambda\epsilon) = \frac{1}{d} \sum_{i=1}^K (\sqrt{d}i^{-\gamma} + \frac{\delta^2}{\sqrt{d}i^{-\gamma}} - \lambda\epsilon)^2, \quad (125)$$

1598 where K is given by $\sqrt{d}K^{-\gamma} + \frac{\delta^2}{\sqrt{d}K^{-\gamma}} - \lambda\epsilon = 0$. Thus we have $K \approx (\sqrt{d}/\lambda\epsilon)^{1/\gamma}$ satisfying
 1599 $1 \ll K < d$. By keeping only the leading terms, we have
 1600

$$1601 \quad J(\delta, \lambda\epsilon) \approx Q^* + \left(\frac{\gamma+1}{\gamma-1} - \frac{1}{2\gamma-1}\right) \left(\frac{\lambda\epsilon}{\sqrt{d}}\right)^{\frac{2\gamma-1}{\gamma}} - \frac{2\lambda\epsilon}{\sqrt{d}} \mathbf{1}_{\gamma>1}, \quad (126)$$

1603 where we use
 1604

$$1605 \quad \sum_{i=1}^K i^{-\gamma} \approx \frac{K^{1-\gamma}}{1-\gamma} + \zeta(\gamma) \mathbf{1}_{\gamma>1} \quad (127)$$

1608 and thus $Q^* := \sum_{i=1}^K i^{-2\gamma} \approx \zeta(2\gamma)$. Taking it into eq. (20), we have
 1609

$$1610 \quad \begin{cases} 4\tilde{\alpha}\delta - \frac{\delta}{\epsilon} = 0 \\ Q^* + \frac{\Delta}{2} + 2\tilde{\alpha}\delta^2 - \frac{\delta^2}{\epsilon} = Q^* - \frac{2\gamma}{2\gamma-1} \left(\frac{\lambda\epsilon}{\sqrt{d}}\right)^{\frac{2\gamma-1}{\gamma}}, \end{cases} \quad (128)$$

1613 which gives $\epsilon = \frac{1}{4\tilde{\alpha}}$ and
 1614

$$1615 \quad R := 2\tilde{\alpha}\delta^2 - \frac{\Delta}{2} = \frac{2\gamma}{2\gamma-1} \left(\frac{\lambda\epsilon}{\sqrt{d}}\right)^{\frac{2\gamma-1}{\gamma}} = \frac{2\gamma}{2\gamma-1} \left(\lambda \frac{d^{3/2}}{4n}\right)^{\frac{2\gamma-1}{\gamma}}. \quad (129)$$

1617 The condition $\max(\delta, d^{-\gamma+1/2}) \ll \lambda\epsilon \ll \sqrt{d}$ gives
 1618

$$1619 \quad \max\left(\sqrt{\frac{n}{d^2}}, \frac{n}{d^{\gamma+\frac{3}{2}}}\right) \ll \lambda \ll \frac{d^{3/2}}{n}. \quad (130)$$

1620 **Phase III: Intermediate over-regularization phase** Phase III is $\delta \ll \lambda\epsilon \ll d^{-\gamma+\frac{1}{2}}$. In this case
 1621 all the spikes are above the cutoff, and all the bulk is below the cutoff. Thus we have
 1622

$$1623 J(\delta, \lambda\epsilon) = \frac{1}{d} \sum_{i=1}^{cd} (\sqrt{d}i^{-\gamma} + \frac{\delta^2}{\sqrt{d}i^{-\gamma}} - \lambda\epsilon)^2 \approx Q^* - \lambda\epsilon c(d)^{\min(\gamma, 1)-1} + \lambda^2\epsilon^2 \quad (131)$$

1626 by eq. (127). Then eq. (20) simplifies to
 1627

$$1628 \begin{cases} 4\tilde{\alpha}\delta - \frac{\delta}{\epsilon} = 0 \\ 1629 Q^* + \frac{\Delta}{2} + 2\tilde{\alpha}\delta^2 - \frac{\delta^2}{\epsilon} = Q^* - \lambda^2\epsilon^2, \end{cases} \quad (132)$$

1630 which gives $\epsilon = \frac{1}{4\tilde{\alpha}}$ and
 1631

$$1632 R := 2\tilde{\alpha}\delta^2 - \frac{\Delta}{2} = \frac{\lambda^2 d^4}{16n^2}. \quad (133)$$

1635 The condition $\delta \ll \lambda\epsilon \ll d^{-\gamma+\frac{1}{2}}$ reduces to
 1636

$$1637 \sqrt{\frac{n}{d^2}} \ll \lambda \ll \frac{n}{d^{\gamma+3/2}}, \quad (134)$$

1639 which further requires $n \gg d^{2\gamma+1}$.
 1640

1641 **Phase IV and V: Benign and harmful overfitting phase** Phase IV and V are $d \ll n \ll d^2$ and
 1642 $0 < 2 - \frac{\lambda\epsilon}{\delta} \ll 1$, $d^{-\gamma+\frac{1}{2}} \ll \delta \ll \sqrt{d}$. In this case the cutoff is close to the boundary of the bulk and
 1643 a part of the spikes are outside the bulk. Thus we have $J(\delta, \lambda\epsilon) \approx J_1(\delta, \lambda\epsilon) + J_2(\delta, \lambda\epsilon)$, where
 1644

$$1645 J_2(\delta, \lambda\epsilon) := \int_{\lambda\epsilon}^{\delta} \mu_{sc}(x/\delta)/\delta(x - \lambda\epsilon)^2 dx \approx \delta^2 \frac{16t^{7/2}}{105\pi} + A\delta^2 t^{9/2} \quad (135)$$

1648 with A a constant, $t := 2 - \frac{\lambda\epsilon}{\delta}$ and
 1649

$$1650 J_1(\delta, \lambda\epsilon) := \frac{1}{d} \sum_{i=1}^{(\delta/\sqrt{d})^{-1/\gamma}} (\sqrt{d}i^{-\gamma} + \frac{\delta^2}{\sqrt{d}i^{-\gamma}} - \lambda\epsilon)^2 \\ 1651 \approx Q^* + \left(\frac{\delta}{\sqrt{d}} \right)^{2-\frac{1}{\gamma}} \left(-\frac{1}{2\gamma-1} + (\lambda\epsilon/\delta)^2 + 2 - 2\frac{\lambda\epsilon}{\delta} \frac{1}{1-\gamma} - \frac{2}{1+\gamma} \frac{\lambda\epsilon}{\delta} + \frac{1}{1+2\gamma} \right) \\ 1652 - \mathbf{1}_{\gamma>1} \zeta(\gamma) \frac{2\lambda\epsilon}{\sqrt{d}}, \quad (136)$$

1658 where we use $\delta \gg d^{-\gamma+\frac{1}{2}}$ to obtain the first line and use eq. (127) for the second line. Then eq.
 1659 (20) simplifies to
 1660

$$1661 \begin{cases} 4\tilde{\alpha}\delta^2 - \frac{\delta^2}{\epsilon} = \delta^2 \frac{16t^{5/2}}{15\pi} + \delta^2 t^{7/2} \left(\frac{32}{105\pi} + 9A \right) \\ 1662 + \left(\left(-\frac{1}{2\gamma-1} + 4 + 2 - \frac{4}{1-\gamma} - \frac{4}{1+\gamma} + \frac{1}{1+2\gamma} \right) (2 - 1/\gamma) + C'(\gamma) \right) \left(\frac{\delta}{\sqrt{d}} \right)^{2-\frac{1}{\gamma}} \\ 1663 Q^* + \frac{\Delta}{2} + 2\tilde{\alpha}\delta^2 - \frac{\delta^2}{\epsilon} = Q^* + \delta^2 \frac{16t^{5/2}}{15\pi} + \delta^2 t^{7/2} \left(\frac{16}{105\pi} + 9A \right) \\ 1664 + \left(-\frac{1}{2\gamma-1} + 4 + 2 - \frac{4}{1-\gamma} - \frac{4}{1+\gamma} + \frac{1}{1+2\gamma} + C'(\gamma) \right) \left(\frac{\delta}{\sqrt{d}} \right)^{2-\frac{1}{\gamma}}, \end{cases} \quad (137)$$

1669 where we use $t \ll 1$ to drop the smaller terms. We also use the shorthand $C'(\gamma) := -4 + \frac{2}{1-\gamma} + \frac{4}{1+\gamma}$.
 1670 The second line subtracted by the first line gives
 1671

$$1672 \frac{\Delta}{2} - 2\tilde{\alpha}\delta^2 = \left(\left(6 - \frac{1}{2\gamma-1} - \frac{4}{1+\gamma} + \frac{1}{1+2\gamma} \right) \frac{1-\gamma}{\gamma} - \frac{4}{\gamma} \right) \left(\frac{\delta}{\sqrt{d}} \right)^{2-\frac{1}{\gamma}} - \delta^2 \frac{16t^{7/2}}{105\pi}. \quad (138)$$

1674 Therefore, at the leading order we have $\delta \approx \sqrt{\frac{\Delta}{4\tilde{\alpha}}}$ and
 1675

$$1676 \quad \delta^2 \frac{16t^{5/2}}{15\pi} \approx 4\tilde{\alpha}\delta^2 - \frac{\delta^2}{\epsilon} \approx \Delta, \quad (139)$$

1677 where we assume $\lambda\delta \ll 1$. Then we have
 1678

$$1680 \quad R := 2\tilde{\alpha}\delta^2 - \frac{\Delta}{2} = \frac{24\gamma^3}{4\gamma^3 + 4\gamma^2 - \gamma - 1} \left(\frac{d\Delta}{4n} \right)^{1-\frac{1}{2\gamma}} + \frac{\Delta}{7} \left(\frac{15\pi}{4} \right)^{2/5} \left(\frac{n}{d^2} \right)^{2/5}. \quad (140)$$

1682 The condition $d \ll n \ll d^2$ and $\lambda\delta \ll 1, 0 < t \ll 1, d^{-\gamma+1/2} \ll \delta \ll \sqrt{d}$ reduces to
 1683

$$1684 \quad \lambda \ll \sqrt{\frac{n}{d^2}} \quad \text{and} \quad d \ll n \ll d^2, \quad (141)$$

1685 where we use $\delta^2 t^{5/2} \approx \Delta - \frac{\lambda\delta}{2}$. Note that under this condition we further have $t \ll 1$ as $\delta \gg 1$.
 1686

1687 **Interpolation peak** The interpolation peak is at $\tilde{\alpha} = \frac{1}{4}$ and $\lambda \ll 1$. The first case of the interpolation peak is $\max(\lambda\epsilon, d^{-\gamma+1/2}) \ll \delta \ll \sqrt{d}$. Then $J(\delta, \lambda\epsilon) \approx J_1(\delta) + J_2(\delta, \lambda\epsilon)$, where
 1688

$$1689 \quad J_1(\delta) := \frac{1}{d} \sum_{i=1}^{cd} \text{ReLU}(\sqrt{di}^{-\gamma} + \frac{\delta^2}{\sqrt{di}^{-\gamma}})^2 \approx Q^* + C(\gamma) \left(\frac{\delta}{\sqrt{d}} \right)^{2-\frac{1}{\gamma}} \quad (142)$$

1690 by eq. (155) and
 1691

$$1692 \quad J_2(\delta, \lambda\epsilon) := \delta^2 \int_{\lambda\epsilon}^2 \mu_{\text{sc}}(x)(x - \lambda\epsilon/\delta)^2 \approx \frac{\delta^2}{2} - \frac{8}{3\pi} \lambda\epsilon\delta. \quad (143)$$

1693 Then eq. (19) reduces to
 1694

$$1695 \quad \begin{cases} 4\tilde{\alpha}\delta^2 - \frac{\delta^2}{\epsilon} = \delta^2 - \frac{8}{3\pi} \lambda\epsilon\delta + C(\gamma)(2 - 1/\gamma) \left(\frac{\delta}{\sqrt{d}} \right)^{2-\frac{1}{\gamma}} \\ Q^* + \frac{\Delta}{2} + 2\tilde{\alpha}\delta^2 - \frac{\delta^2}{\epsilon} = Q^* + \frac{1}{2}\delta^2 + C(\gamma) \left(\frac{\delta}{\sqrt{d}} \right)^{2-\frac{1}{\gamma}}. \end{cases} \quad (144)$$

1696 By using $\tilde{\alpha} = \frac{1}{4}$, we obtain
 1697

$$1698 \quad \epsilon = \frac{\Delta}{2} \lambda^{-2/3} \left(\frac{3\pi}{8} \right)^2, \quad \delta = \left(\frac{3\pi\Delta^2}{32} \right)^{1/3} \lambda^{-1/3} \quad (145)$$

1699 as the leading order solution, where the $\left(\frac{\delta}{\sqrt{d}} \right)^{2-\frac{1}{\gamma}}$ term is ignored because $\frac{\delta}{\sqrt{d}} \ll 1$. Then we have
 1700

$$1701 \quad R := 2\tilde{\alpha}\delta^2 - \frac{\Delta}{2} \approx 2 \left(\frac{3\pi\Delta^2}{32} \right)^{2/3} \lambda^{-2/3}. \quad (146)$$

1702 The condition $\max(\lambda\epsilon, d^{-\gamma+1/2}) \ll \delta \ll \sqrt{d}$ reduces to
 1703

$$1704 \quad d^{-3/2} \ll \lambda \ll 1 \quad (147)$$

1705 The second case of the interpolation peak is $\max(\lambda\epsilon, \sqrt{d}) \ll \delta$, which gives $J(\delta, \lambda\epsilon) \approx \frac{\delta^2}{2} - \frac{8}{3\pi} \lambda\epsilon\delta$.
 1706 Similarly we can obtain the solution
 1707

$$1708 \quad \epsilon = \left(Q^* + \frac{\Delta}{2} \right) \lambda^{-2/3} \left(\frac{3\pi}{8} \right)^2, \quad \delta = \left(\frac{3\pi}{8} \right)^{1/3} \left(Q^* + \frac{\Delta}{2} \right)^{2/3} \lambda^{-1/3} \quad (148)$$

1709 and thus
 1710

$$1711 \quad R := 2\tilde{\alpha}\delta^2 - \frac{\Delta}{2} \approx 2 \left(\frac{3\pi}{8} \right)^{2/3} \left(Q^* + \frac{\Delta}{2} \right)^{4/3} \lambda^{-2/3}. \quad (149)$$

1712 The condition $\max(\lambda\epsilon, \sqrt{d}) \ll \delta$ reduces to
 1713

$$1714 \quad \lambda \ll d^{-3/2}. \quad (150)$$

Phase VI: Large-sample phase The first case of Phase VI is $n \gg d^2$ and $\lambda\epsilon \ll \delta \ll d^{-\gamma+\frac{1}{2}}$. In this case the cutoff is almost 0 and all spikes are outside the bulk. Then we have $J(\delta, \lambda\epsilon) = Q^* + \frac{1}{2}\delta^2$, and thus eq. (20) simplifies to

$$\begin{cases} 4\tilde{\alpha}\delta - \frac{\delta}{\epsilon} = \delta \\ Q^* + \frac{\Delta}{2} + 2\tilde{\alpha}\delta^2 - \frac{\delta^2}{\epsilon} = Q^* + \frac{1}{2}\delta^2, \end{cases} \quad (151)$$

which has a solution

$$\delta^2 = \frac{\Delta}{4\tilde{\alpha} - 1}, \quad \epsilon = \frac{1}{4\tilde{\alpha} - 1}. \quad (152)$$

Then we have

$$R := 2\tilde{\alpha}\delta^2 - \frac{\Delta}{2} \approx \frac{\Delta}{8\tilde{\alpha}} \quad (153)$$

for $\tilde{\alpha} \gg 1$ and the condition $\lambda\epsilon \ll \delta \ll d^{-\gamma+\frac{1}{2}}$ reduces to

$$\lambda \ll \sqrt{\frac{n}{d^2}} \quad \text{and} \quad n \gg d^{2\gamma+1}. \quad (154)$$

The second case of Phase IV is $d^2 \ll n \ll d^{2\gamma+1}$ and $\max(\lambda\epsilon, d^{-\gamma+\frac{1}{2}}) \ll \delta \ll \sqrt{d}$. In this case the cutoff is almost 0 but only a part of the spikes are outside the bulk. Thus we have $J(\delta, \lambda\epsilon) = J_1(\delta) + \frac{1}{2}\delta^2$, where

$$\begin{aligned} J_1(\delta) &:= \frac{1}{d} \sum_{i=1}^{cd} \text{ReLU}(\sqrt{d}i^{-\gamma} + \frac{\delta^2}{\sqrt{d}i^{-\gamma}})^2 \\ &\approx \frac{1}{d} \sum_{i=1}^{(\delta/\sqrt{d})^{-1/\gamma}} (\sqrt{d}i^{-\gamma} + \frac{\delta^2}{\sqrt{d}i^{-\gamma}})^2 \\ &= Q^* + C(\gamma) \left(\frac{\delta}{\sqrt{d}} \right)^{2-\frac{1}{\gamma}}, \end{aligned} \quad (155)$$

where $C(\gamma)$ is some constant. In the second line we use $\delta \gg d^{-\gamma+1/2}$. In the third line we use eq. (127) and only keep the leading term. Then eq. (20) reduces to

$$\begin{cases} 4\tilde{\alpha}\delta^2 - \frac{\delta^2}{\epsilon} = \delta^2 + C(\gamma)(2 - 1/\gamma) \left(\frac{\delta}{\sqrt{d}} \right)^{2-\frac{1}{\gamma}} \\ Q^* + \frac{\Delta}{2} + 2\tilde{\alpha}\delta^2 - \frac{\delta^2}{\epsilon} = Q^* + \frac{1}{2}\delta^2 + C(\gamma) \left(\frac{\delta}{\sqrt{d}} \right)^{2-\frac{1}{\gamma}} \end{cases} \quad (156)$$

The second equation subtracted by the first equation gives

$$\frac{\Delta}{2} - 2\tilde{\alpha}\delta^2 = -\frac{1}{2}\delta^2 - C(\gamma)(1 - 1/\gamma) \left(\frac{\delta}{\sqrt{d}} \right)^{2-\frac{1}{\gamma}}. \quad (157)$$

As $n \gg d^2$, at the leading order we have $\delta \approx \sqrt{\frac{\Delta}{4\tilde{\alpha}}}$. Then one can verify that if $n \ll d^{2\gamma+1}$ we have $\left(\frac{\delta}{\sqrt{d}} \right)^{2-\frac{1}{\gamma}} \ll \delta^2$, which suggests that

$$R := 2\tilde{\alpha}\delta^2 - \frac{\Delta}{2} \approx \frac{1}{2}\delta^2 \approx \frac{\Delta}{8\tilde{\alpha}}. \quad (158)$$

In this case we also have $\epsilon \approx \frac{1}{4\tilde{\alpha}}$, and thus the condition $\max(\lambda\epsilon, d^{-\gamma+\frac{1}{2}}) \ll \delta \ll \sqrt{d}$ reduces to

$$\lambda \ll \sqrt{\frac{n}{d^2}} \quad \text{and} \quad d^2 \ll n \ll d^{2\gamma+1}. \quad (159)$$

To conclude, Phase VI is

$$R \approx \frac{\Delta d^2}{8n}, \quad \text{if} \quad n \gg d^2 \quad \text{and} \quad \lambda \ll \sqrt{\frac{n}{d^2}}. \quad (160)$$

1782 C.4 UNIVERSAL ERROR DECOMPOSITION OF FEATURE LEARNING
1783

1784 In this section we derive Result 3. As a part of the spikes are outside the bulk and a part of the spikes
1785 are inside (e.g., in phases IV and V), we can rewrite the SE as

$$1786 \begin{cases} 4\tilde{\alpha}\delta^2 - \frac{\delta^2}{\epsilon} = \delta\partial_\delta(J_1(\delta, \lambda\epsilon) + J_2(\delta, \lambda\epsilon)) \\ 1787 Q^* + \frac{\Delta}{2} + 2\tilde{\alpha}\delta^2 - \frac{\delta^2}{\epsilon} = (1 - \lambda\epsilon\partial_{\lambda\epsilon})(J_1(\delta, \lambda\epsilon) + J_2(\delta, \lambda\epsilon)), \end{cases} \quad (161)$$

1789 where the auxiliary functions are defined as

$$1790 \quad 1791 \quad 1792 \quad J_1(\delta, \lambda\epsilon) := \frac{1}{d} \sum_{i=1}^{K(\delta)} (s_i + \frac{\delta^2}{s_i} - \lambda\epsilon)^2, \quad (162)$$

1793 and

$$1794 \quad 1795 \quad 1796 \quad J_2(\delta, \lambda\epsilon) := \delta^2 \int_{\lambda\epsilon/\delta}^2 \mu_{\text{sc}}(x)(x - \lambda\epsilon/\delta)^2. \quad (163)$$

1797 Recall we are considering a general model with s_i denoting the i -th eigenvalue in a descending
1798 order and $K(\delta) \ll d$ satisfying $p_{K(\delta)} + \frac{\lambda^2}{p_{K(\delta)}} - \lambda\epsilon = 0$. The excess risk is given by

$$1799 \quad 1800 \quad R := 2\tilde{\alpha}\delta^2 - \frac{\Delta}{2} = Q^* + (\delta\partial_\delta + \lambda\epsilon\partial_{\lambda\epsilon} - 1)(J_1(\delta, \lambda\epsilon) + J_2(\delta, \lambda\epsilon)). \quad (164)$$

1801 Then we have

$$1802 \quad 1803 \quad (\delta\partial_\delta + \lambda\epsilon\partial_{\lambda\epsilon} - 1)J_1(\delta, \lambda\epsilon) = \frac{2}{d} \sum_{i=1}^{K(\delta)} (s_i + \frac{\delta^2}{s_i} - \lambda\epsilon)(\frac{2\delta^2}{s_i} - \lambda\epsilon) - \frac{1}{d} \sum_{i=1}^{K(\delta)} (s_i + \frac{\delta^2}{s_i} - \lambda\epsilon)^2 \\ 1804 \quad 1805 \quad = \frac{1}{d} \sum_{i=1}^{K(\delta)} \left[(\frac{\delta^2}{s_i} - \lambda\epsilon)^2 + \frac{\delta^2}{s_i}(s_i + \frac{\delta^2}{s_i} - \lambda\epsilon) \right] - \frac{1}{d} \sum_{i=1}^{K(\delta)} s_i^2. \quad (165)$$

1806 and

$$1807 \quad 1808 \quad (\delta\partial_\delta + \lambda\epsilon\partial_{\lambda\epsilon} - 1)J_2(\delta, \lambda\epsilon) = \delta^2 \int_{\lambda\epsilon/\delta}^2 \mu_{\text{sc}}(x)(x - \lambda\epsilon/\delta)^2. \quad (166)$$

1809 Now we obtain eq. (17) by using $Q^* := \frac{1}{d} \sum_{i=1}^d s_i^2$.

1810 C.5 PERTURBATIVE EXPANSION OF THE BULK
1811

1812 In this session we discuss how to obtain the correction of the bulk in eq. (98). Consider $H :=$
1813 $Z + \sum_{i=1}^k \lambda_i v_i v_i^T$ with $\{\lambda_i\}_{i=1}^k$ smaller than 1, where $Z \sim \text{GOE}(d)$ and $\{v_i\}_{i=1}^k$ are uniformly
1814 sampled from the unit sphere. Its resolvent can be expanded as

$$1815 \quad 1816 \quad m_H(z) := \frac{1}{d} \text{Tr}(z - H)^{-1} \\ 1817 \quad 1818 \quad \approx m_Z(z) + \frac{1}{d} \sum_{i=1}^k \lambda_i v_i^T (z - Z)^{-2} v_i + \frac{1}{d} \sum_{i,j=1}^k \text{Tr}(z - Z)^{-1} v_i v_i^T (z - Z)^{-1} v_j v_j^T (z - Z)^{-1}. \\ 1819 \quad 1820 \quad (167)$$

1821 For the first-order correction we have $\frac{1}{d} \sum_{i=1}^k \lambda_i v_i^T (z - Z)^{-2} v_i \approx \frac{\sum_{i=1}^k \lambda_i}{d} m'_Z(z)$. For the second-
1822 order correction we have

$$1823 \quad 1824 \quad \frac{1}{d} \sum_{i,j=1}^k \text{Tr}(z - Z)^{-1} v_i v_i^T (z - Z)^{-1} v_j v_j^T (z - Z)^{-1} \\ 1825 \quad 1826 \quad \approx \frac{\text{Tr}(z - Z)^{-1} \text{Tr}(z - Z)^{-2} + \text{Tr}(z - Z)^{-3}}{d^2(d+2)} \sum_{i=1}^k \lambda_i^2 \\ 1827 \quad 1828 \quad \approx -\frac{1}{d} \sum_{i=1}^k \lambda_i^2 m_Z(z) m'_Z(z). \quad (168)$$

1836 This gives a correction on the spectrum $\tilde{\nu}(x) = \frac{\sum_{i=1}^k \lambda_i}{d} \mu'_{\text{sc}}(x) - \frac{\sum_{i=1}^k \lambda_i^2}{d} \text{im}(m_Z(x + i0)m'_Z(x + i0))$. Note that the first term is an odd function and the second term is an even function, and the
 1837 resolvent of GOE is given by
 1838

$$1840 \quad m_Z(x + i0) = \frac{x}{2} + i\mu_{\text{sc}}(x), \quad (169)$$

1841 so we have
 1842

$$\begin{aligned} 1843 \quad \frac{4\pi^2}{3} \int \nu_H(x)^3 dx &\approx \frac{4\pi^2}{3} \int \mu_{\text{sc}}(x)^3 dx + 4\pi^2 \int \mu_{\text{sc}}(x)^2 \tilde{\nu}(x) dx \\ 1844 \quad &= 1 - \left(\frac{1}{d} \sum_{i=1}^k \lambda_i^2 \right) 2\pi^2 \int \mu_{\text{sc}}(x)^2 (x\mu'_{\text{sc}}(x) + \mu_{\text{sc}}(x)) dx \\ 1845 \quad &= 1 - \left(\frac{1}{d} \sum_{i=1}^k \lambda_i^2 \right) \frac{4\pi^2}{3} \int \mu_{\text{sc}}(x)^3 dx \\ 1846 \quad &= 1 - \frac{1}{d} \sum_{i=1}^k \lambda_i^2. \\ 1847 \quad & \\ 1848 \quad & \\ 1849 \quad & \\ 1850 \quad & \\ 1851 \quad & \\ 1852 \quad & \\ 1853 \quad & \end{aligned} \quad (170)$$

1854 This correction is the leading term only if $\sum_{i=1}^k \lambda_i^2 \ll \sum_{i=1}^k \lambda_i^2$. However, if $\lambda_i = i^{-\gamma}$, all the
 1855 higher-order terms are of the same order, but their sum converges for $|z| > 3$, which gives
 1856

$$1857 \quad \frac{4\pi^2}{3} \int \nu_H(x)^3 dx = 1 - \Theta \left(\frac{1}{d} \sum_{i=1}^k \lambda_i^2 \right) \quad (171)$$

1860 instead.
 1861

D COMPARISON WITH L_2 REGULARIZATION

1864 In this section we compare the scaling laws we have obtained for ERM to the ones of ridge regression
 1865 for a linear model, proving in particular their sub-optimality. The ridge estimator is defined as
 1866

$$1867 \quad \hat{\boldsymbol{\theta}}_{\text{ridge}} = \arg \min_{\boldsymbol{\theta} \in \mathbb{R}^d} \frac{1}{n} \sum_{\mu=1}^n (y_\mu - \langle \boldsymbol{\theta}, \mathbf{x}_\mu \rangle)^2 + \lambda \|\boldsymbol{\theta}\|_2^2. \quad (172)$$

1870 This can be mapped to both the diagonal network and quadratic network case, depending on the
 1871 choice of \mathbf{x} . For simplicity, we assume $\mathbf{x} \sim \mathcal{N}(0, I_d)$.

1872 Cheng & Montanari (2024) readily implies the following.
 1873

1874 **Theorem 2** (Excess risk rates for ridge regression). . Assume that $y = \langle \boldsymbol{\theta}^*, \mathbf{x} \rangle + \sqrt{\Delta} \zeta$ with $\zeta \sim$
 1875 $\mathcal{N}(0, 1)$ and $\mathbb{E}[\|\boldsymbol{\theta}^*\|_2^2] = \Theta(1)$. For $n, d \gg 1$, the excess risk associated to the estimator defined in
 1876 (172) satisfies

$$1877 \quad R_{n,d} = \Theta \begin{cases} 1, & \text{if } n \ll d \text{ or } \lambda \gg 1, \\ 1878 \quad \lambda^2, & \text{if } n \gg d \text{ and } \sqrt{d/n} \ll \lambda \ll 1 \\ 1879 \quad \Delta d/n, & \text{if } n \gg d \text{ and } \lambda \ll \sqrt{d/n} \\ 1880 \quad \Delta \lambda^{-1/2}, & \text{if } n = d \text{ and } \lambda \ll 1. \end{cases} \quad (173)$$

1882 *Proof.* The excess risk concentrates with high probability, for $n, d \gg 1$, around the following deterministic expression (Cheng & Montanari, 2024)

$$1885 \quad R_{n,d} = \frac{n\nu^2}{n(1+\nu)^2 - d} \mathbb{E}[\|\boldsymbol{\theta}^*\|_2^2] + \frac{d\Delta}{n(1+\nu)^2 - d} \quad (174)$$

1887 with ν the unique non-negative solution of
 1888

$$1889 \quad \frac{n}{d} \left(1 - \frac{\lambda}{\nu} \right) = \frac{1}{1+\nu}. \quad (175)$$

1890 Therefore

$$\nu = \Theta \begin{cases} d/n + \lambda, & \text{if } n \ll d, \\ \lambda, & \text{if } n \gg d, \\ \sqrt{\lambda}, & \text{if } n = d \text{ and } \lambda \ll 1. \end{cases} \quad (176)$$

1895 Substituting into (174), the result follows. \square 1896 Therefore, we cannot obtain a non-trivial risk for $n \ll d$ with L_2 regularization.

1899 E NUMERICAL DETAILS

1901 The state equations (20) can be iterated in a more numerically convenient form that depends on an
 1902 extended set of parameters $(q, m, \Sigma, \hat{q}, \hat{m}, \hat{\Sigma})$ as presented in [Erba et al. \(2025\)](#), Appendix A.4.4.
 1903 Then, we can compute δ and ϵ as $\delta = \sqrt{\hat{q}}/\hat{m}$ and $\epsilon = 2/\hat{m}$. Since the limiting distribution of S^* is
 1904 not easy to compute exactly as $d \rightarrow \infty$, we compute the integral J by a Monte-Carlo procedure. The
 1905 overlaps m, q, Σ are computed using finite size samples of matrices and their eigen-decomposition

$$M = \sqrt{\hat{q}}Z + \hat{m}S^* = O \text{ diag}(\nu_1, \dots, \nu_d)O^T \quad (177)$$

1908 where $Z \sim \text{GOE}(d)$ and $S^* = \frac{\sqrt{d}}{\sum_i i^{-2\gamma}} \text{ diag}(1, 2^{-\gamma}, \dots, d^{-\gamma})$ can be taken as a diagonal matrix,
 1909 since this amounts to a rotation of M , which does not affect the distribution of Z by rotational
 1910 invariance. One can then apply the spectral denoiser described in [Erba et al. \(2025\)](#) and compute the
 1911 overlaps using the reconstructed matrix $\tilde{M} = O \text{ diag}(\tilde{\nu}_1, \dots, \tilde{\nu}_d)O^T$, where $\tilde{\nu}_i = \frac{1}{\Sigma} \text{ ReLu}(\nu_i - 2\lambda)$
 1912 are the denoised eigenvalues. Finally, the order parameters can be computed as
 1913

$$\begin{cases} m^{t+1} = \frac{1}{d} \mathbb{E}_M \text{ Tr}[(S^*)^T \tilde{M}] \\ q^{t+1} = \frac{1}{d} \mathbb{E}_M \text{ Tr}[\tilde{M}^T \tilde{M}] \\ \Sigma^{t+1} = \frac{2}{d} \mathbb{E}_M \left[\sum_{i=1}^d \frac{\Theta(\nu_i - 2\lambda)}{\Sigma} + \sum_{i < j} \frac{\tilde{\nu}_i - \tilde{\nu}_j}{\nu_i - \nu_j} \right] \end{cases} \quad (178)$$

1918 The expectation is taken over $n_{samples} = \Theta(10)$ samples for $d = \Theta(10^2)$, independently for each
 1919 order parameter, for a total of $3n_{samples}$ sampled matrices per iteration of the state evolution.
 1920

1921 Since the ERM problem is convex we resort to using LBFGS with Wolfe line search. We used
 1922 the PyTorch implementation of the optimiser, taking care of evaluating the network efficiently at
 1923 each pass. For the specifics of the implementation we refer to the code included in the submission.
 1924 Convergence is typically achieved with a precision of at least 10^{-8} in a few hundred iterations. The
 1925 main challenge is in storing the dataset in memory. For each run we used up to 1800 gigabytes
 1926 of RAM on nodes with 2 Intel Xeon 8360Y CPUs. Our total computing cost (including initial
 1927 explorations) is around 200000 CPU hours.
 1928
 1929
 1930
 1931
 1932
 1933
 1934
 1935
 1936
 1937
 1938
 1939
 1940
 1941
 1942
 1943